

Photogenerated high-density electron-hole plasma energy relaxation and experimental evidence for rapid expansion of the electron-hole plasma in CdSe

Mahesh R. Junnarkar and R. R. Alfano

Institute for Ultrafast Spectroscopy and Lasers, Department of Physics, The City College of New York, New York, New York 10031

(Received 21 January 1986)

The kinetics of the nonequilibrium photogenerated electron-hole plasma in CdSe is investigated using picosecond time-resolved spectroscopy at room temperature. Based on the fact that the polar optical-phonon emission rate is reduced due to screening by the high density of the e - h plasma, the remaining dominant mechanism for hot-carrier cooling is the nonpolar optical-phonon emission even though CdSe is a highly polar semiconductor. It has been observed that the photogenerated carrier density is much lower than the estimated carrier density using known values of the absorption coefficient, reflectivity, and photon fluence. Rapid plasma expansion has been proposed as a possible explanation on the grounds of the observed larger spatial width of the photoluminescence relative to the laser spatial width, moderate change of Auger recombination rate with the excitation fluence, the absence of an observed change in the Fermi level with increased excitation intensity, and earlier formation of excitons after the picosecond pulse (5 psec) excitation at a low temperature (12 K). The observed carrier density ≈ 35 psec after excitation is limited to $1 \times 10^{19} \text{ cm}^{-3}$ within the excitation photon fluence of $2 \times 10^{15} - 7 \times 10^{16}$ photons/cm² at room temperature. Large values of the diffusion constant are explained in terms of a screened electron-phonon interaction. The possibility of saturation of the available states in explaining small carrier densities is eliminated by the observed faster cooling rate at low-excitation intensity and the sublinear change in the luminescence spatial width with excitation fluence.

I. INTRODUCTION

The photogeneration of an electron-hole (e - h) plasma in semiconductors has been studied¹⁻³ for many years. Probing this plasma in time provides valuable information on both the nonequilibrium and equilibrium states in terms of the interaction among elementary excitations with the environment, mainly the lattice. The knowledge obtained from these studies are relevant to laser annealing processes in semiconductors. The carriers created from the absorption of a laser photon at energy $\hbar\omega_l$ ($\hbar\omega_l > E_g$), where E_g is the band gap, are hot having a pseudotemperature given by⁴ $T_i \approx \frac{1}{3}(\hbar\omega_l - E_g)/k_B$. Due to carrier-carrier scattering ($\approx 10^{-14}$ sec) it is assumed that the electron and hole system each have the same temperature. In our experiment, with CdSe and $\hbar\omega_l = 2.34$ eV, the carrier pseudotemperature is ≈ 2560 K. The primary channels for energy relaxation of these hot carriers are carrier-carrier scattering, plasmon production, and phonon emission. Of these processes, all but phonon emission primarily involve the redistribution of the carrier energy among the electrons and holes with negligible amounts of energy transferred to the lattice. In a semiconductor, the optical-phonon energy is typically ≈ 25 meV, while the acoustical phonon energy is much smaller. Therefore, the energy relaxation process is dominated by optical-phonon emission as long as the carrier kinetic energy is larger than the optical-phonon energy. The rest of the kinetic energy is dissipated as acoustical phonons. An excellent review of these processes is given by Yoffa⁵ and Nag.⁶ Generally, the energy relaxation rates are carrier-density dependent. For a hot-electron (hole) having excess kinetic

energy E , the energy-loss rate per carrier due to collisions with the N other electrons (holes) is given by⁷

$$\frac{dE}{dt} = - \frac{4\pi N e^2}{\epsilon_0^2 (2m_e E)^{1/2}}, \quad (1)$$

where e and m_e are the electron (hole) charge and effective mass, and ϵ_0 is the bulk dielectric constant. This N -dependent energy relaxation rate causes rapid thermalization of photogenerated carriers within $\approx 10^{-14}$ sec. The plasmon frequency is dependent on carrier density ($\omega_p \sim \sqrt{N}$). The energy relaxation process involving LO phonons can be effectively screened at high carrier densities and this subject will be discussed later. The first steady-state experimental observation of carrier heating in CdSe was reported by Shah *et al.*² at an estimated photogenerated carrier density of $2 \times 10^{16} \text{ cm}^{-3}$. Free e - h plasma expansion has been observed in CdSe at 4 K by Cornet *et al.*⁸ Their observation by analyzing spectra emitted from different photoexcited regions showed that the velocities are two orders of magnitude greater than the thermodynamic equilibrium diffusion velocity. However, they did not observe any plasma expansion at room temperature. They reasoned that the absence of a large number of thermal phonons at low temperatures made it possible to observe this expansion only at low temperatures. Combescot *et al.*⁹ have calculated diffusion velocities at $T = 0$ K, using a hydrodynamic model. The velocities suggested by this model are $\approx 10^8$ cm/sec. It is also possible to calculate the velocities by considering^{8,10} the pressure developed when the e - h plasma density is above the e - h liquid density ($5.4 \times 10^{17} \text{ cm}^{-3}$). The large pressure generated causes rapid diffusion of free carriers. The

pressure is given by $p = N[\partial F/\partial d \ln(n)]|_{T, \tilde{N}}$, where \tilde{N} is the total number of e - h pairs, N is the carrier density, and F is the free energy per pair. The plasma expansion has also been observed in GaAs (Ref. 11) and in GaAs_{1-x}P_x (Ref. 12) at 2 K. Forchel *et al.*¹³ have pointed out the significant effect of carrier drift velocities on the transmission and emission spectra of a rapidly diffusing nonequilibrium e - h plasma in semiconductors. These examples indicate that the presence of fast diffusion and the consequent reduction in carrier density can play an important role in various energy relaxation processes.

The purpose of our research is twofold: to experimentally demonstrate the rapid diffusion of photogenerated carriers in CdSe from the photoexcitation region at both room and low temperatures and to show the role of partially screened nonpolar optical-phonon emission in the cooling of high-density hot carriers and in the rapid diffusion of these carriers.

II. BACKGROUND

A. Electron-phonon interaction and carrier temperature relaxation

It has been shown by Yoffa¹⁴ that the electron- (hole) lattice (polar and nonpolar) interaction which results in emission of LO phonons could be effectively screened for carrier densities greater than the critical density N_c , which is a characteristic of a particular semiconductor. In direct-gap polar semiconductors like CdSe or GaAs the intravalley polar transitions are dominant in terms of hot-carrier energy relaxation at low-carrier densities ($N < N_c$). A typical scattering rate^{5,14} in this situation is 1×10^{11} eV/sec. The critical density associated with such transitions (polar and nonpolar) is given by

$$N_c = \frac{\epsilon_0 \hbar q^3}{8\pi e^2} \frac{1}{(\beta m_e)^{1/2}}. \quad (2)$$

In CdSe this equation can be simplified to $N_c = 1.5 \times 10^{-4} (T_e q^3)^{1/2}$, where q is the phonon wave vector and $\beta = 1/k_B T_e$, where T_e is the carrier temperature. In polar semiconductors, the polar electron-phonon interaction is governed by matrix element^{15,16} $V \approx 1/q$. Thus, the phonons with large q do not participate much in the interaction. Considering a parabolic conduction band in a semiconductor, one would like to see a range of q 's of phonons emitted during the energy relaxation process via LO-phonon emission. The Fig. (1) shows the relaxation of a hot-electron via intravalley LO-phonon emission. The minimum phonon wave vector that can couple two conduction band states occurs when the direction of the electron wave vector is unchanged. The maximum wave vector is created when the electron momentum direction is reversed. The values of q_{\min} and q_{\max} are weakly dependent on the initial electron density and can be calculated from the band structure. Without screening the created phonons are not evenly distributed¹⁷ between q_{\min} and q_{\max} because of the inverse q^2 factor in the Fröhlich interaction. The values of q_{\min} and q_{\max} are calculated at the point of excitation in the E - k band-structure diagram.

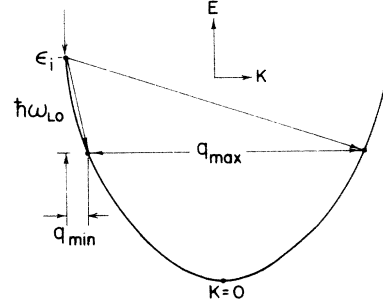


FIG. 1. Parabolic band structure around $k=0$ is shown with initial energy ϵ_i ($t=0$). The phonon q vectors involved in one LO-phonon emission are shown as q_{\min} and q_{\max} .

For a semiconductor with band gap E_g and laser photon energy $\hbar\omega$, the initial kinetic energy of electrons before thermalization is given by

$$E_e = (\hbar\omega - E_g) \frac{m_h}{m_h + m_e}, \quad (3)$$

where m_e and m_h are the effective masses of electrons and holes, respectively. Since the electrons and holes are assumed to be in thermal equilibrium $T_e = T_h$ (e - e and e - h scattering time $\approx 10^{-14}$ sec), the initial e - h plasma temperature during the laser pulse (width ≈ 5 psec) will be

$$T_i = \frac{1}{3k_B} (\hbar\omega_i - E_g) \quad \text{and} \quad E_i = \frac{3}{2} k_B T_i. \quad (4)$$

It can be easily shown that the minimum and maximum q values for LO-phonon energy δ is given by

$$q_{\min} = (2m_e)^{1/2} [(E_i)^{1/2} - (E_i - \delta)^{1/2}] (1/\hbar) \quad (5)$$

and

$$q_{\max} = (2m_e)^{1/2} [(E_i)^{1/2} + (E_i - \delta)^{1/2}] (1/\hbar) \quad (6)$$

for the conduction band, respectively. Similarly, values can be obtained for the valence band. Using Eqs. (4), (5), and (6) for CdSe with the values $0.13m_0$, 2.34 eV, 1.71 eV, and 26 meV of the electron effective mass, excitation laser photon energy, band gap, and LO-phonon energy, the carrier temperature is $T_i = 2560$ K, $E_i = 0.32$ eV, $q_{\min} \approx 4.6 \times 10^5$ cm⁻¹, and $q_{\max} \approx 2.2 \times 10^7$ cm⁻¹.

From Eq. (2) the critical density N_c corresponding to q_{\min} is 7×10^{14} cm⁻³, while the critical density corresponding to q_{\max} is 8×10^{19} cm⁻³. These values should only be used as a guideline since the q_{\max} decreases with time during the energy relaxation process and hence the corresponding N_c will decrease with time. However, it is possible to calculate N_c if the carrier temperature is experimentally known.

In order to calculate the density of photogenerated carriers produced by a laser pulse, we should first consider the density of states¹⁸ at the point of excitation. For a parabolic band the number of energy states per unit volume between the interval E and $E + dE$ is given by

$$N(E) dE = \frac{1}{2\pi^2 \hbar^3} (2m_e)^{3/2} (\sqrt{E}) dE. \quad (7)$$

Since the laser photon spectral width and band warping are 20 meV, $dE = 20$ meV and $E_e = 0.489$ eV. Thus, $N(E)dE = 1.3 \times 10^{19} \text{ cm}^{-3}$. The total density of states integrated from 0 up to E_i is $7 \times 10^{19} \text{ cm}^{-3}$. The e - e scattering time⁵ τ_{e-e} is $\approx 10^{-14}$ sec and the pulse width is 5 psec. The total carrier density could be as high as $6.5 \times 10^{21} \text{ cm}^{-3}$, if we take into account all the indirect valleys (equivalents of X and L). Because the scattering time out of the states being 10^{-14} sec is faster than the pump duration of 5 psec, the conduction state could be occupied and emptied 500 times ($5 \times 10^{-12}/10^{-14}$) during the laser pulse. Most of the zinc-blende-type semiconductors like GaAs or CdTe have indirect L and X valleys with an indirect band gap $\approx E_g + 0.3$ eV. The local symmetry of the wurtzite crystal structure is very similar to zinc blende. It is reasonable to assume the existence of indirect valleys. As far as the electron- (hole) phonon interaction is concerned the total carrier density, irrespective of valleys, plays a role in the screening of this interaction. With our range of photon fluence $7 \times 10^{16} (I_F) - 2 \times 10^{15} (\frac{1}{33} I_F)$ photon/cm², a range of carrier densities $3 \times 10^{21} - 8.5 \times 10^{19} \text{ cm}^{-3}$ can be estimated if one uses a reflectivity coefficient [refractive index ≈ 2.6 (Ref. 19)] $R = 0.2$ and an absorption coefficient²⁰ $\alpha = 5 \times 10^4 \text{ cm}^{-1}$ (for one-photon absorption) in the expression

$$N = (1-R)I\alpha \text{ cm}^{-3}. \quad (8)$$

This expression does not take into account any diffusion during the laser pulse duration nor any recombination. In this case the estimated carrier density range of

$3 \times 10^{21} - 8.5 \times 10^{19} \text{ cm}^{-3}$ is below the saturation limit of $6.5 \times 10^{21} \text{ cm}^{-3}$.

The phonon emission rate per carrier can be written as¹⁴

$$\nu = \frac{\nu_0}{1 + (N/N_c)^2}. \quad (9)$$

ν_0 is the unscreened phonon emission rate and incorporates the Frölich interaction term ($1/q^2$) for polar interaction and is independent of q for nonpolar interaction. The phonon emission rate depends on the carrier density and can be estimated from the delay time of band-edge luminescence. It can be seen that the q_{\min} polar phonon emission is completely screened for a carrier density in the range $3 \times 10^{21} - 8.5 \times 10^{19} \text{ cm}^{-3}$ ($N_c \sim 1 \times 10^{15} \text{ cm}^{-3}$). But a q_{\max} for phonon emission cannot be screened until the carrier density reaches a value above $8 \times 10^{19} \text{ cm}^{-3}$. However, the $1/q^2$ dependence for the polar emission probability (incorporated in ν_0) decreases the emission rate by a factor of ≈ 1370 over unscreened q_{\min} phonon emission. The net effect is that all the intravalley polar LO-phonon emission processes are screened and cannot contribute to the hot-carrier energy relaxation mechanism for $N > 10^{15} \text{ cm}^{-3}$ on the picosecond time scale. The phonon emission frequencies for polar and nonpolar interactions for q_{\min} and q_{\max} are plotted with the carrier density N in Fig. 2. The emission frequencies show a dramatic reduction for carrier densities exceeding the respective critical densities N_c .

Since the polar phonon emission are most likely

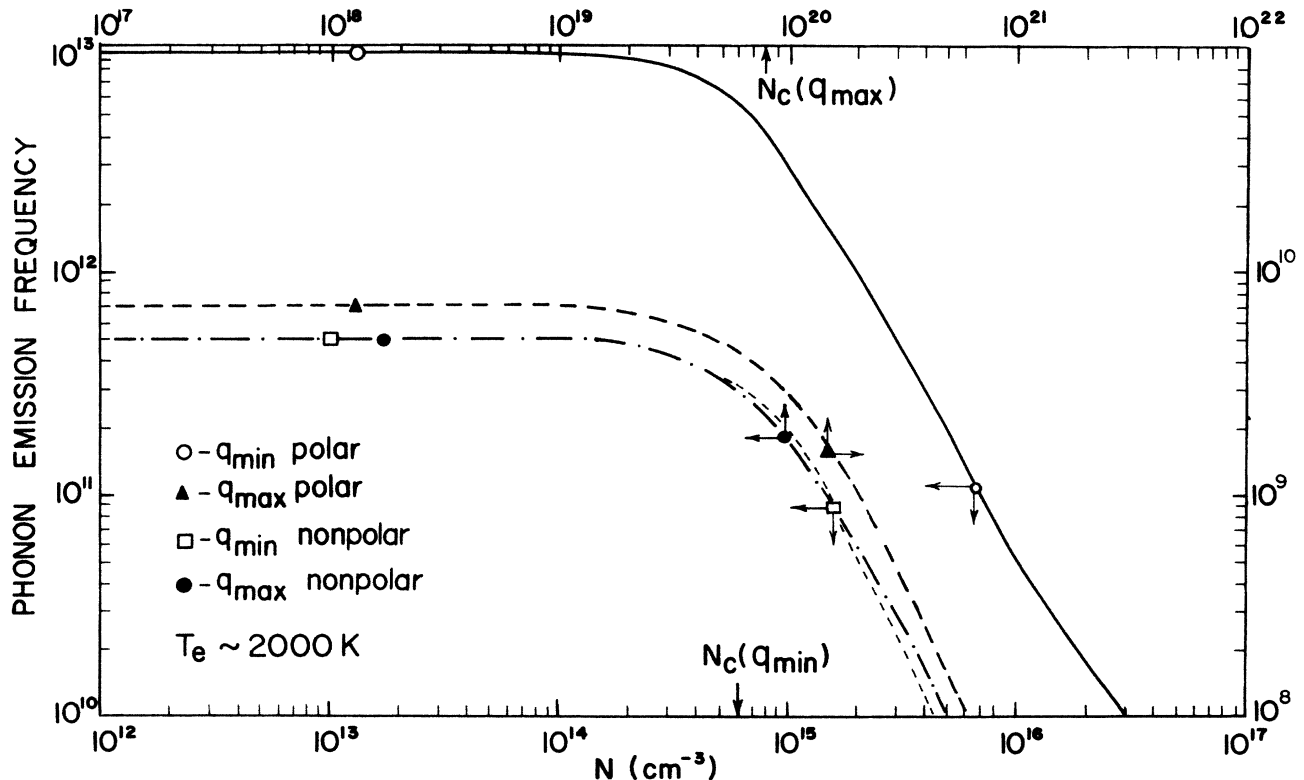


FIG. 2. Phonon emission frequencies for polar and nonpolar interactions and q_{\min} and q_{\max} are plotted as a function of carrier density. N_c 's are the critical densities for polar and nonpolar phonon scattering.

screened, the next dominant mechanism for energy relaxation of hot conduction electrons (valence holes) is due to LO-phonon emission via nonpolar optical-phonon scattering. This process is also known as optical deformation potential scattering.¹⁶ In the case of nonpolar interactions, the optical-phonon emission does not in general depend on the phonon wave vector. The nonpolar optical matrix element has been shown¹⁶ to be almost independent of q with a small higher-order dependence on the wave vector of the phonon. This type of scattering is similar to acoustical phonon scattering except that a fixed quantum of energy $\hbar\omega_0$ (or δ) (LO-phonon energy) is emitted for all q 's.

The theory developed by Yoffa¹⁴ for electron optical-phonon screening holds equally for polar and nonpolar phonons in terms of the critical carrier-density calculation [Eq. (2)]. Thus, nonpolar phonon emission with wave vector q_{\max} and critical density $N_c = 8 \times 10^{19} \text{ cm}^{-3}$, would dominate the energy relaxation process, while q_{\min} emission is completely screened for the relevant carrier densities ($10^{19} - 10^{21} \text{ cm}^{-3}$) in our experiments (Fig. 2).

The average rate of change of carrier energy due to nonpolar optical interactions for a Maxwell-Boltzmann distribution of carriers at temperature T_e is given by¹⁶

$$\frac{dE}{dt} = - \left[\frac{\sqrt{2}}{\sqrt{\pi}} \right] \left[\frac{D'^2(m_e)^{3/2}}{\pi \hbar^2 \rho} \right] (k_B T_e)^{1/2} \beta(x_0, x_e), \quad (10)$$

where

$$\beta(x_0, x_e) = \frac{\exp(x_0 - x_e) - 1}{\exp(x_0) - 1} \left[\frac{x_e}{2} \right] \exp \left[\frac{x_e}{2} \right] \times K_1 \left[\frac{x_e}{2} \right],$$

with

$$x_0 = \frac{\delta}{k_B T_0}, \quad x_e = \frac{\delta}{k_B T_e}.$$

T_0 is the lattice temperature, K_1 is a Bessel function of the second kind [$K_1(x_e/2) \approx 2/x_e$ for small x_e], and D' is the conduction-band deformation potential.^{16,21,22} Equation (10) gives $T_e(t)$ and the temperature relaxation rate of hot carriers.

B. Luminescence for high excitation

The photoexcited carriers (e - h) recombine during the process of thermalization. The recombination photoluminescence is characterized by carrier temperature, carrier density (Fermi energy), and the band gap of the semiconductor. This allows us to make a reasonable estimate of the carrier density and carrier temperature T_e by studying either time-resolved luminescence within different spectral bands (streak camera) or time-resolved spectra (with time gate). An estimate of the average carrier density and temperature can be obtained from a time-integrated spectrum within the dynamic range limited time interval (in our case, 100–800 psec to be explained later) of the detection system.

In semiconductors at ultrahigh photogenerated carrier densities, the third-order nonradiative band-to-band Auger mechanism,²³ can dominate all other recombi-

tion processes such as radiative and surface recombination, and trapping at crystal defects. The cubic dependence²³ on carrier density in addition to the linear term arises from the three-body character of the Auger process, whereby an electron recombines with a hole, and the excess energy is transferred to another electron or a hole in the form of kinetic energy.

The equation for the time dependence of carrier density $N(t)$ for Auger recombination of carriers is given by²³

$$\frac{dN(t)}{dt} = -CN^3(t) - \frac{N(t)}{\tau}, \quad (11)$$

where C is the Auger recombination constant and τ is the total recombination lifetime of free carriers. For high-density e - h plasma luminescence intensity $L(t) \approx N(t)P(t) \approx [N(t)]^2$. Hence, for $B'/2 = C$ and $2\tau' = \tau$, the equation (11) can be rewritten for the time dependence of luminescence intensities as

$$\frac{dL(t)}{dt} = -B'[L(t)]^2 - \frac{L(t)}{\tau'}, \quad (12)$$

where τ' is the luminescence lifetime. The solution to Eq. (12) is given by

$$L(t) = \frac{L(0)}{[1 + L(0)B'\tau'] \exp(t/\tau') - L(0)B'\tau'}. \quad (13)$$

The luminescence time-resolved data can provide values of carrier density if the values of $\frac{1}{2}L(0)B'$ are obtained using Eq. (13) (see Fig. 15) and if the Auger recombination constant is known [$N^2(0)C = B'/2L(0)$]. It has been shown that the pure collision Auger process is almost negligible in comparison with the phonon-assisted Auger recombination over a wide temperature ($> 100 \text{ K}$) and for carriers with densities $\approx 10^{19} \text{ cm}^{-3}$ on a psec scale. Takeshima *et al.*²⁴ have calculated the Auger recombination coefficient C for GaAs $\approx 10^{-29} \text{ cm}^{-6} \text{ sec}^{-1}$ taking into account screening of free-carrier phonon interactions. We have assumed $C \approx 1 \times 10^{-29} \text{ cm}^{-6} \text{ sec}^{-1}$ at 1000 K. We have used this value of C to estimate the carrier density.

In direct-gap semiconductors nonmomentum conserving transitions²⁵ can connect states having different k directions provided the emitted phonon has a large momentum but small energy. At high-carrier temperature $\approx 1000 \text{ K}$, the acoustical phonon emission rate is $\approx 10^{10} \text{ eV/sec}$ in CdSe [Eq. (40)]. Hence, considering an upper limit for an acoustical phonon of 1 meV (and $k \approx 10^7 \text{ cm}^{-1}$) the corresponding phonon emission time is of the order of 0.1 psec. During the lifetime ($\approx 100 \text{ psec}$) of a free carrier, the acoustical phonon emission is highly probable and the luminescence spectra will correspond to non- k -selection transitions. In this case the luminescence intensities will depend on the electron and hole density of states separately. The emission arises from k rings at fixed energies ϵ_e and ϵ_h . This is in contrast to the conventional non- k -selection transition²⁵ which allows for large-carrier energies requiring integration over $\epsilon_e(\epsilon_h)$. The large-energy phonon emission probability is small compared to the small-energy phonon. This type of momentum relaxed non- k -selection transition gives us the best theoretical fits.

In this case the emission spectrum $L(\epsilon)$, taking into ac-

count the Fermi distribution of both electrons and holes, and the respective density of states is given by

$$L(\epsilon) = A(\epsilon_e)^{1/2}(\epsilon_h)^{1/2} \{ \exp[(\epsilon_e - \mu_e)/k_B T_e] + 1 \} \\ \times \{ \exp[(\epsilon_h - \mu_h)/k_B T_e] + 1 \} \quad (14)$$

where ϵ_e , ϵ_h are the free energies of electrons and holes, respectively, measured from the respective band edges; μ_e and μ_h are the Fermi energies for electrons and holes measured from the respective band edges; T_e is the common temperature assigned to the e - h plasma; and ϵ is the photoluminescence photon energy corresponding to an ϵ_e , ϵ_h energy pair.

The expression given above [Eq. (14)] is simplified further using the relationships

$$\epsilon = \epsilon_e + \epsilon_h + E_g, \quad (15)$$

$$\epsilon_e = \left[\frac{\epsilon - E_g}{m_e + m_h} \right] m_h, \quad (16)$$

$$\epsilon_h = \left[\frac{\epsilon - E_g}{m_e + m_h} \right] m_e, \quad (17)$$

$$L(\epsilon) = A(\epsilon - E_g) / \{ \exp[(\epsilon - E_g)\mu/m_e - \mu_e]/k_B T_e + 1 \}^{-1} \{ \exp[(\epsilon - E_g)\mu/m_h - \mu_h]/k_B T_e + 1 \}^{-1}. \quad (22)$$

By substituting Eq. (21) into Eq. (22), the luminescence spectrum can be expressed in terms of conduction electron parameters as

$$L(\epsilon) = A(\epsilon - E_g) / \{ \exp[(\epsilon - E_g)\mu/m_e - \mu_e]/k_B T_e + 1 \}^{-1} \{ \exp[(\epsilon - E_g)\mu/m_h - \mu_e m_e/m_h]/k_B T_e + 1 \}^{-1}. \quad (23)$$

The carrier density is estimated from curve fitting using the Fermi-level energy parameter and carrier temperature parameter.

The carrier density is given by²³

$$N = N'_c f_{1/2}(\eta), \quad (24)$$

where $\eta = \mu_e/k_B T_e$ and

$$N'_c = 4.831 \times 10^{15} (m_e/m_0)^{3/2} T_e^{3/2} \text{ cm}^{-3}.$$

For a wide range of $\eta \geq 1$ it has been shown,²³ within 3% error, that

$$f_{1/2}(\eta) \approx \left[\frac{4\eta(\frac{3}{2})}{3\pi(\frac{1}{2})} \right] \left[1 + \frac{\pi^2}{8\eta^2} \right], \quad (25)$$

where

$$f_{1/2}(\eta) = \int_0^\infty (E/k_B T_e)^{1/2} (dE/k_B T_e) \\ \times [1 + \exp(E - \eta)/k_B T_e]^{-1}. \quad (26)$$

Using the known values of band gap of 1.71 eV (724 nm) at lattice temperature (300 K), the theoretical fits to the luminescence spectra for various excitation powers were obtained (Figs. 12 and 13). The carrier temperature and Fermi level are used as variable parameters. The low-energy edge of the luminescence spectra is sensitive to the choice of Fermi-level values, while the high-energy edge is sensitive to the choice of temperature values. The carrier density and T_e obtained from this analysis is an average within time interval 100–800 psec.

where m_e and m_h are the effective masses for electrons and holes. Furthermore,

$$\epsilon_e = \frac{(\epsilon - E_g)\mu}{m_e}, \quad (18)$$

$$\epsilon_h = \frac{(\epsilon - E_g)\mu}{m_h}, \quad (19)$$

where μ is the reduced mass for electron and hole and

$$\frac{1}{\mu} = \frac{1}{m_e} + \frac{1}{m_h}. \quad (20)$$

Since the electron and hole density are the same ($N = n_e = n_h$), assuming all the preferential traps (n or p type) are screened at the high e - h plasma density, the Fermi energies are related by

$$\frac{\mu_e}{\mu_h} = \frac{m_h}{m_e}, \quad (21)$$

where μ_e and μ_h are the Fermi energies for electrons and holes, respectively [and $N \approx (m_{e(h)}\mu_{e(h)})^{3/2}$]. Thus, $L(\epsilon)$ can be written as

C. Hot- and high-density-carrier diffusion

The photogenerated or electrically injected carriers diffuse into the bulk of a semiconductor even in the absence of an electric field due to their thermal velocities, band bending, and intrinsic collisions. It has been pointed out by Yoffa *et al.*²⁶ that at high photogeneration rates the laser energy given to the lattice within a characteristic depth is determined primarily by carrier diffusion.

The ambipolar diffusion constant D_0 is given by²⁶

$$D_0 \approx \frac{2k_B T_e \tau_e \tau_h}{m_e \tau_h + m_h \tau_e}, \quad (27)$$

where τ_e and τ_h are collision times and depend on carrier and lattice temperatures. For unscreened impurity scattering $\tau_{0_i} \approx \tau_{0_h}$ is about 10^{-13} sec and for hot-carrier temperature of 2000 K, $D_{0_i} = 105 \text{ cm}^2/\text{sec}$. For unscreened nonpolar optical-phonon scattering τ_{0_p} is 2×10^{-12} sec [Eq. (10)] at $T_e = 2000 \text{ K}$, yielding $D_{0_p} \approx 2100 \text{ cm}^2/\text{sec}$.

The continuity equation which governs the carrier density in space (x) and time (t) for the one-dimensional case in the absence of electric fields, for low-carrier density, and δ -function-type photoexcitation is given by²⁷

$$\frac{\partial N}{\partial t} = -\frac{N}{\tau} + D_0 \left[\frac{\partial^2 N}{\partial x^2} \right], \quad (28)$$

where τ is the total lifetime of a free carrier. The solution to the above equation is given by²⁷

$$N(x,t) = \frac{N'}{(4\pi D_0 t)^{1/2} [\exp(-t/\tau - x^2/4D_0 t)]}, \quad (29)$$

where $N' = N/\alpha$, assuming a small optical absorption depth ($\alpha \approx 5 \times 10^4 \text{ cm}^{-1}$) and N is given by Eq. (8). During a typical delay time of ≈ 30 psec observed in our experiments and a lifetime of 400 psec, the reduction in the carrier density is only by a factor of 10. In order to explain the observed (see Secs. II A, II B, II C, and II D) larger changes in the carrier density one needs a large diffusion constant which is at least $100D_0$. Since the diffusion constant depends on a particular scattering mechanism via τ_e , one should take into account the screening effect on that scattering mechanism due to the presence of a high-density e - h plasma.

The enhancement of the ambipolar diffusion constant D_0 for large densities has been pointed out by Frigo *et al.*²⁸ Accordingly, the carrier diffusion at low temperature is dominated by impurity scattering. By treating the impurities as ionized centers whose Coulomb potential is screened by the carrier plasma, an effective diffusion coefficient can be determined²⁸ by using elementary kinetic theory and the Born approximation. For densities greater than Mott density N_M ($1 \times 10^{17} \text{ cm}^{-3}$), this approach yields a density-dependent diffusion coefficient,²⁸

$$D_i = D_{0i} (N/N_m)^\alpha, \quad (30)$$

where $D_{0i} = 105 \text{ cm}^2/\text{sec}$ (τ_{0i} for impurity scattering $\approx 10^{-13} \text{ sec}$ and $T_e \approx 2000 \text{ K}$) and $\alpha = \frac{4}{3}$ for ambipolar diffusion and full-carrier screening. At high densities the potential is more effectively screened so that the carriers diffuse rapidly away from the surface. For the lower densities the impurities become more efficient scatterers and make the diffusion coefficient decrease with density.

At high-carrier densities, as we have seen earlier [Eq. (9)], the LO-phonon-carrier scattering time becomes longer,

$$\tau_p = \tau_{0p} \left[1 + \left(\frac{N}{N_c} \right)^2 \right]. \quad (31)$$

Therefore using τ_p and Eq. (27), the phonon-assisted carrier diffusion constant becomes

$$D_p = D_{0p} \left[1 + \left(\frac{N}{N_c} \right)^2 \right]. \quad (32)$$

The total diffusion constant due to impurity and phonon scattering is given by

$$D_t = \frac{D_i D_p}{D_i + D_p} = \frac{D_{0i} D_{0p} (N/N_m)^\alpha [1 + (N/N_c)^2]}{D_{0i} (N/N_m)^\alpha + D_{0p} [1 + (N/N_m)^2]}. \quad (33)$$

A plot of D_t versus N is shown in Fig. 3 for $D_{0i} = 105 \text{ cm}^2/\text{sec}$, $D_{0p} = 2100 \text{ cm}^2/\text{sec}$, $T_e = 2000 \text{ K}$, $\tau_{0i} = 10^{-13} \text{ sec}$, $\tau_{0p} = 2 \times 10^{-12} \text{ sec}$, $N_m = 1 \times 10^{17} \text{ cm}^{-3}$, and $N_c = 8 \times 10^{19} \text{ cm}^{-3}$. The salient features of the plot are, for $N < 10^{19} \text{ cm}^{-3}$, the diffusion constant increases slowly, while for $N > 10^{19} \text{ cm}^{-3}$, the diffusion constant in-

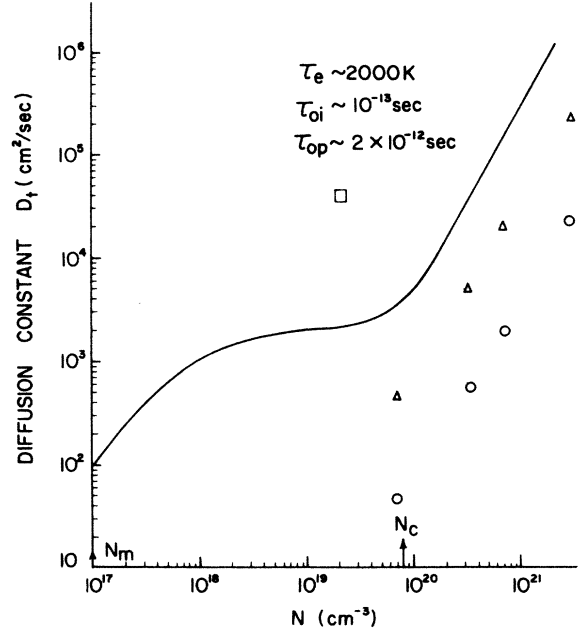


FIG. 3. Diffusion constant obtained by considering screened impurity and nonpolar phonon scattering of carriers is plotted as a function of carrier density. N_m and N_c are the critical densities for screened impurity and nonpolar optical-phonon scattering. The carrier temperature and unscreened values of collision times are given in the figure. \circ and \triangle represent experimental values for $C = 1 \times 10^{-29} \text{ cm}^{-6} \text{ sec}^{-1}$ and $1 \times 10^{-28} \text{ cm}^{-6} \text{ sec}^{-1}$, respectively. \square represents diffusion constant obtained from exciton formation data.

creases rapidly and becomes extremely large. Thus, at very high densities the mean collision time becomes very large which removes the barrier for carrier expansion.

III. SAMPLES

The samples used in this study were CdSe(1) with the c -axis perpendicular to the plane and CdSe(3) with the c -axis parallel to the plane. These samples were obtained from Cleveland Crystals. The crystals were of high resistivity and were grown by the vapor phase method and their surfaces were chemically etched.

IV. EXPERIMENTAL METHODS

The samples CdSe(1) and CdSe(3) were chosen to see if any difference would exist at room temperature in the e - h recombination kinetics²⁹ due to the participation of different valence bands. In the excitation process of CdSe(1), the holes are generated in the $\Gamma_9(A)$ and $\Gamma_7(B)$ valence bands. In CdSe(3), due to the orientation of the c axis parallel to the excitation photon polarization, the holes are generated only in the $\Gamma_7(B)$ valence band.

For the experiments at low temperature (12 K), the sample was mounted on a cold finger, in an optical Dewar, with a Si diode mounted behind it to measure the temperature. Otherwise, the samples were mounted on a glass plate for room-temperature experiments.

Photoexcited carriers were produced using a Nd:glass

mode locked³⁰ laser. A single pulse of 1060-nm wavelength was selected using a spark gap and Pockel cell. The pulse width was about 5–6 psec. The pulse selected³⁰ at the 1060-nm wavelength was frequency doubled to 530 nm for one-photon excitation experiments. For two-photon excitation, the 1060-nm wavelength was selected. The pulse intensity was attenuated using calibrated neutral density filters. The maximum energy per pulse at 530 nm was 400 μJ with an excitation spot size of 1.35 mm diameter (photon fluence $\approx 7 \times 10^{16}$ photons/cm²). The maximum energy per pulse at 1060 nm was 1200 μJ with an excitation spot size of 1.9 mm diameter (photon fluence $\approx 2 \times 10^{17}$ photons/cm²).

For the time-resolved luminescence study, the luminescence was collected, collimated, and focused onto a 50- μm slit of a streak camera. The luminescence was selected in broadbands with combinations of filters (HOYA R68 passes 680–720 nm and the HOYA R65-DITRICH SHP680 combination passes 640–680-nm wavelengths). A prepulse was set (530 nm original pulse) by using a beam splitter, which would arrive at the streak camera about 110 psec prior to the beginning of luminescence. This was done in order to measure the delay times of the luminescence accurately. The total delay between the peak of the time-resolved luminescence and the excitation pulse was calculated taking into account the optical path length added to the excitation and to the luminescence path by the various combination of filters. The prepulse was also used as a marker for overlapping various data files for averaging. The data was stored in a Digital 11-03 computer and analyzed later.

The time-integrated spectra was obtained using a $\frac{1}{4}$ meter Spex spectrometer coupled to a vidicon intensified target (PAR OMA II). The grating used had 300 grooves/mm blazed at 500 nm. The spectral resolution of the system was 30 Å. The spectra obtained were corrected for S-20 spectral response, pixel response, thermal background, and grating blaze, using the 1216 console (PAR OMA II) microprocessor of the system. The corrected data were then stored and transferred to a Digital 11-03 computer for analysis.

The time-integrated spatial profiles of the laser pulse and luminescence were obtained using a streak camera in the focus mode with input slit removed. Each channel of the video system was calibrated (mm versus channel number) by using an illuminated scale at the sample site.

Excitation laser intensities at 530 nm transmitted through neutral-density filters 0ND, ND25, ND13, and ND3 filters correspond to excitation photon fluences I_F , $\frac{1}{4}I_F$, $\frac{1}{8}I_F$, and $\frac{1}{33}I_F$, respectively, where $I_F = 7 \times 10^{16}$ photons/cm². For the 1060-nm excitation wavelength, the transmission of ND25 is only 10%.

V. EXPERIMENTAL RESULTS

The rise times and decay times for the band-edge luminescence (710 nm) were measured for both samples as a function of excitation fluence at room temperature. The formation time of the excitonic state at 12 K and time-integrated spectra were measured in order to get an estimate of the photogenerated carrier density as a function

of excitation photon fluence. The spatial widths of the 710-nm luminescence were measured as a function of photon fluence to investigate transverse diffusion of carriers from the photoexcited region. These various experimental results are summarized in the following sections.

A. Delay- and decay-time measurements

The time-resolved luminescence at various excitation fluences from CdSe(1) and CdSe(3) are displayed in Figs. 4 and 5, respectively. These curves typically show a laser prepulse and luminescence rising rapidly (≈ 20 psec) and decaying slowly (≈ 230 psec) in time. The rise times [Fig. 4, curves (b)–(e)] were obtained using the expression

$$L(t) = A [\exp(-t/\tau') - \exp(-t/\tau_r)], \quad (34)$$

where τ' and τ_r are the decay and rise times for the time-resolved luminescence, respectively. In Fig. 4 curve (a) corresponds to the zero time, as it only shows the laser prepulse (530 nm) scattered from the sample. The rise times measured for curves (b)–(e) corresponding to CdSe(1) are 20, 17, 16, and 13 psec, respectively. For the entire range of excitation fluence the decay times for 710-nm lumines-

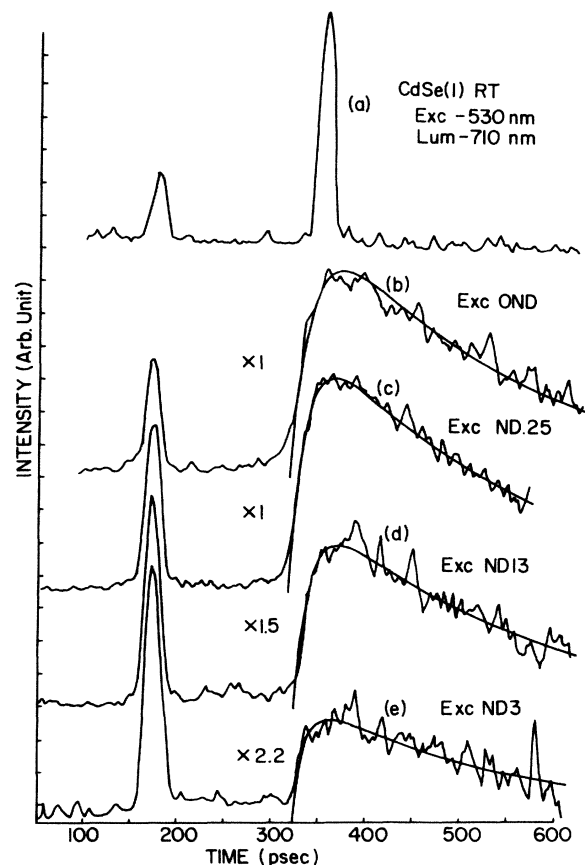


FIG. 4. Time-resolved band-edge photoluminescence at 710 nm from CdSe(1) for various excitation fluences is shown. The decay time for all the curves is 230 psec. The rise times for various curves are (b) 20 psec, (c) 17 psec, (d) 16 psec, and (e) 13 psec, respectively. The curve (a) corresponds to the laser pulse scattered from the sample to provide time zero for accurate determination of delay times [see Eq. (34) for fits].

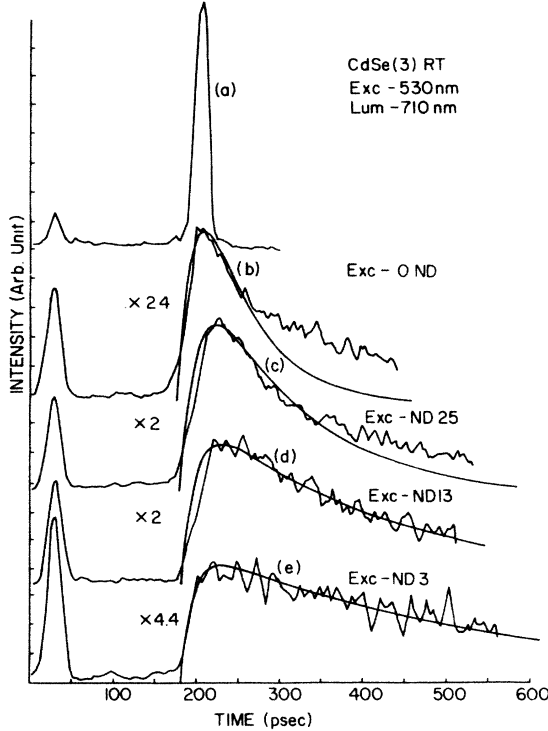


FIG. 5. Time-resolved band-edge photoluminescence at 710 nm from CdSe(3) for various excitation fluences is shown. The rise times for various curves are as follows: (b) 18 psec, (c) 19 psec, (d) 17 psec, and (e) 15 psec, respectively. Curve (a) represents the laser pulse scattered from the sample to provide zero time for accurate determination of delays. The decay times were used only for convenience to obtain the rise times and have no physical significance [see Eq. (34) for fits].

cence is ≈ 230 psec. The delay times of the band-edge luminescence (710 nm) for CdSe(1), under a range of photon fluence (I_F to $\frac{1}{33}I_F$), decreases from 46 to 27 psec. The total delay times and fluences are displayed in Table I. The delay times are corrected for the optical delay due to various filters in the path.

In Fig. 5 the rise times measured for curves (b)–(e) corresponding to CdSe(3) are 18, 19, 17, and 15 psec, respectively. In this case, the theoretical fitting is poor since the luminescence is assumed to be monomolecular in the extraction even though there is clearly a fast (35 psec) and a slow (230 psec) component. This behavior was seen for excitation polarizations both parallel and perpendicular to the c axis (accessible by rotating the sample about the excitation axis and keeping the c axis within the same plane). The rise and delay times observed for CdSe(3) are similar to the one observed in CdSe(1) (see Table I). The rise times are of the order of ≈ 20 psec while the delays are ≈ 35 psec.

The luminescence maximum [$dL(t)/dt=0$] occurs at a time $\Delta t'$ measured with respect to the arrival of the excitation pulse at the sample and is given by

$$\Delta t' = \left[\frac{1}{\tau'_r} - \frac{1}{\tau'} \right] \ln \left[\frac{\tau'}{\tau'_r} \right]. \quad (35)$$

TABLE I. Delays between the luminescence maximum and the excitation pulse at the samples are shown for CdSe(1) and CdSe(3) for various excitation fluences. These delays are corrected for the optical delays introduced by excitation and luminescence path filters.

CdSe(1)		CdSe(3)	
Excitation intensity	Delay (psec)	Excitation intensity	Delay (psec)
I_F	46	I_F	50
$\frac{1}{4}I_F$	34	$\frac{1}{4}I_F$	32
$\frac{1}{8}I_F$	38	$\frac{1}{8}I_F$	35
$\frac{1}{33}I_F$	27	$\frac{1}{33}I_F$	35

For typical values of $\tau'_r=20$ psec and $\tau'=230$ psec, $\Delta t'=53$ psec. It is easy to measure $\Delta t'$ experimentally with high accuracy. The values of τ'_r obtained by curve fitting are sensitive to the fittings at large times, the starting point, and shape. Therefore, the delay times are a good measure of the average energy relaxation time Δt ($L(t) \approx [N(t)]^2$ and the luminescence maximum corresponds to the maximum carrier density $N(\Delta t)$ as $\Delta t = \Delta t'$) and should be taken as the average energy relaxation time measured experimentally.

B. Measurement of carrier temperature decay

In order to measure carrier temperatures at different time intervals, the hot luminescence decay profiles (660 nm) and band-edge luminescence decay profiles (710 nm) were obtained at various excitation fluences in CdSe(1) (Figs. 6 and 7) and in CdSe(3) (Figs. 8, 9, 10, and 11). The hot luminescence lifetimes are shorter than the band-edge luminescence which indicates rapid temperature changes at earlier times.

The method used to calculate the temperatures at different time intervals is described as follows. For a Maxwell-Boltzmann distribution of the photogenerated carriers one can evaluate the hot-carrier-energy relaxation rate from the ratio of hot luminescence to band-edge luminescence intensities as a function of time. The inverse carrier temperature T_e at time t after the excitation pulse is given by

$$\frac{1}{T_e(t)} = - \left[\frac{k_B}{E_{\text{hot}} - E_{\text{BE}}} \right] \left[\frac{R(t)}{R(t_1)} \right] + \frac{1}{T_1}, \quad (36)$$

where E_{hot} and E_{BE} are the hot and band-edge luminescence photon energies. [In our case, they correspond to 660 nm (1.875 eV) and 710 nm (1.743 eV), respectively]; T_1 is measured from the time-integrated spectra and corresponds to the lattice temperature within 100–700 psec; $R(t)$ is the ratio of intensities of hot and band-edge luminescence at time t ; $R(t_1)$ is the corresponding ratio when the temperature T_1 is reached after 200 psec. Measurements of T_1 are discussed in Sec. V C.

In Figs. 6 and 7, (a) shows the hot (660 nm), while the curve (b) shows the band-edge (710 nm) luminescence decay profiles for CdSe(1). The excitation and luminescence polarizations are perpendicular to the c axis. The tem-

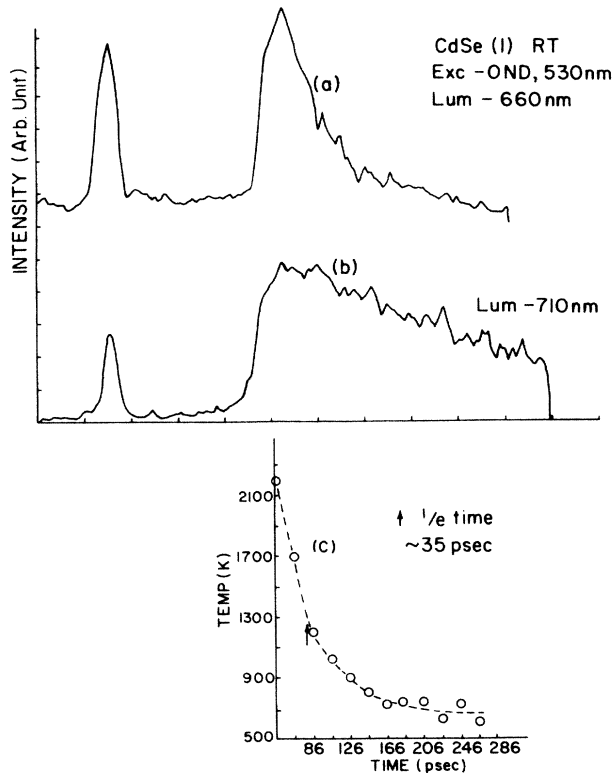


FIG. 6. Curves (a) and (b) represent hot (660 nm) and band-edge (710 nm) luminescence from CdSe(1) at photon fluence I_F . The temperature decay profile is calculated using Eq. (36).

peratures at 20-psec intervals [Fig. 6(c)] were obtained by a method described earlier. For the maximum excitation (I_F) the initial temperature of ≈ 2200 K goes down to 1200 K within ≈ 35 psec ($1/e$ time). For weak excitation ($\frac{1}{33}I_F$), the cooling rate is smaller ($1/e$ time ≈ 100 psec) and the initial temperature is ≈ 700 K (Fig. 7).

For CdSe(3), the temperature cooling times are smaller (rates are larger) for comparable excitation fluences as compared to CdSe(1). In Figs. 8, 9, 10, and 11, curve (a) correspond to hot luminescence decay profiles for excitation fluences I_F , $\frac{1}{4}I_F$, $\frac{1}{8}I_F$, and $\frac{1}{33}I_F$, respectively. Curve (b) corresponds to band-edge luminescence for the same range of photon excitation fluence. The corresponding curves for temperatures versus time in psec are shown in Figs. 8(c), 9(c), 10(c), and 11(c), respectively. The initial temperatures obtained for photon fluences I_F , $\frac{1}{4}I_F$, $\frac{1}{8}I_F$, and $\frac{1}{33}I_F$, are 2200, 1800, 1800, and 1300 K, respectively. The temperature decay times are 30, 35, 35, and 60 psec, respectively. The excitation polarization in this case was parallel to the c axis, while the luminescence polarization was both parallel and perpendicular to the c axis. All the initial temperatures obtained correspond to times given in Table I.

C. Measurement of time-integrated spectra

The time-integrated spectra for CdSe(1) obtained at room temperature are shown in Fig. 12 for various photon

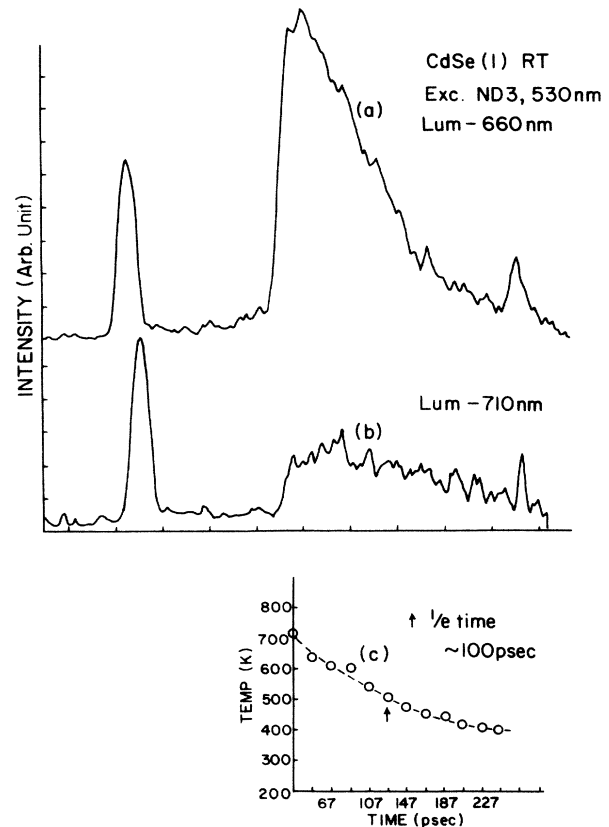


FIG. 7. Curves (a) and (b) represent hot (660 nm) and band-edge (710 nm) luminescence from CdSe(1) at photon fluence $\frac{1}{33}I_F$. The temperature decay profile is calculated using Eq. (36).

fluences. The luminescence shows a high-energy tail and an almost cutoff at low-energy side. These measurements were made to obtain an average Fermi energy (hence carrier density) for a given excitation fluence. The carrier density is calculated to be $\approx 5 \times 10^{18} \text{ cm}^{-3}$ for the photon excitation fluence range I_F to $\frac{1}{33}I_F$ (Table II). The carrier temperature range for the time duration of 100–800 psec is estimated to be 600–400 K for the respective excitation fluences.

Similar results were obtained for CdSe(3) (see Fig. 13). The carrier density in this case is $\approx 7.5 \times 10^{18} \text{ cm}^{-3}$ and the temperature range for the time duration (100–800 psec) is 800–500 K for the excitation fluence range $I_F - \frac{1}{33}I_F$ (Table III).

D. Measurement of exciton formation time

The free $e-h$ plasma time resolved band-edge photoluminescence from CdSe(3) at 12 K is displayed in Fig. 16, curve (a). The luminescence is delayed from the excitation pulse by ≈ 20 psec at most. The lifetime corresponding to the decay ($1/e$) is ≈ 120 psec. In Fig. 16 curve (b) corresponds to excitonic luminescence (see discussion in Sec. VIII C) at the lowest two-photon excitation fluence. The peak of the luminescence matches with the peak of the free $e-h$ luminescence peak in curve (a) of

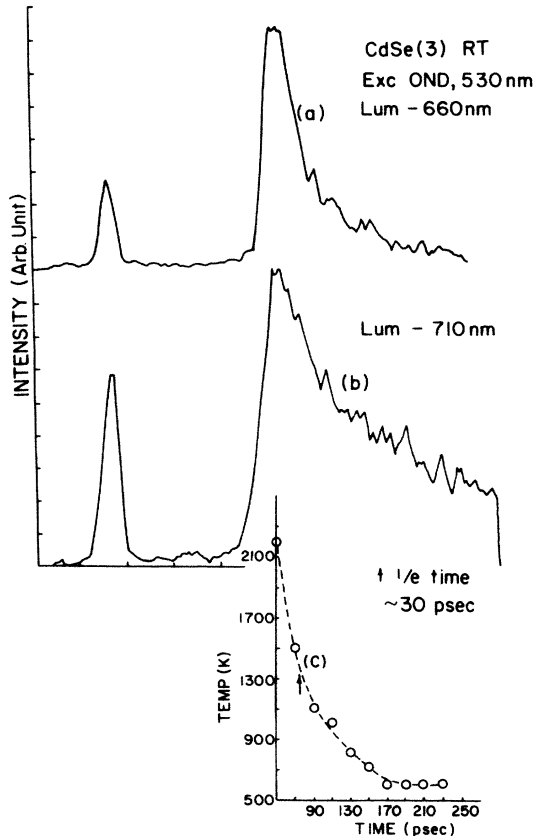


FIG. 8. Curves (a) and (b) represent hot (660 nm) and band-edge (710 nm) luminescence from CdSe(3) at photon fluence I_F . The temperature decay profile is obtained from Eq. (36).

Fig. 16. The exciton peak, however, shifts to larger times with excitation [Fig. 16, curves (b)–(d)] and for the maximum two-photon excitation it is delayed by 185 psec [Fig. 16, curve (d)]. The free e - h plasma luminescence cannot be observed due to the low quantum yield (lower by a factor of 250). A check for stimulated emission, by studying the luminescence intensity versus excitation fluence, confirmed its absence.

E. Measurement of luminescence spatial profiles

In order to examine the existence of transverse diffusion of carriers, the luminescence spatial profiles at the samples (luminescence spot diameter) were measured. The laser spatial profile of a 530-nm pulse at the sample site is shown by curve (a) of Fig. 17 with FWHM of 1.35 mm. The band-edge luminescence profile at the sample is about 2.19 mm wide (FWHM) for an excitation fluence of $\frac{1}{33}I_F$ [Fig. 17, curve (b)] while for larger excitation at I_F the spot profile is still larger ≈ 3.14 mm [Fig. 17, curve (c)]. The profiles observed were time integrated over a time period of 1 nsec (dynamic range limited time) on a streak camera in the focus mode.

VI. DISCUSSION

In this section the delay times and the decay times will be analyzed to obtain the energy relaxation rates.⁵ The

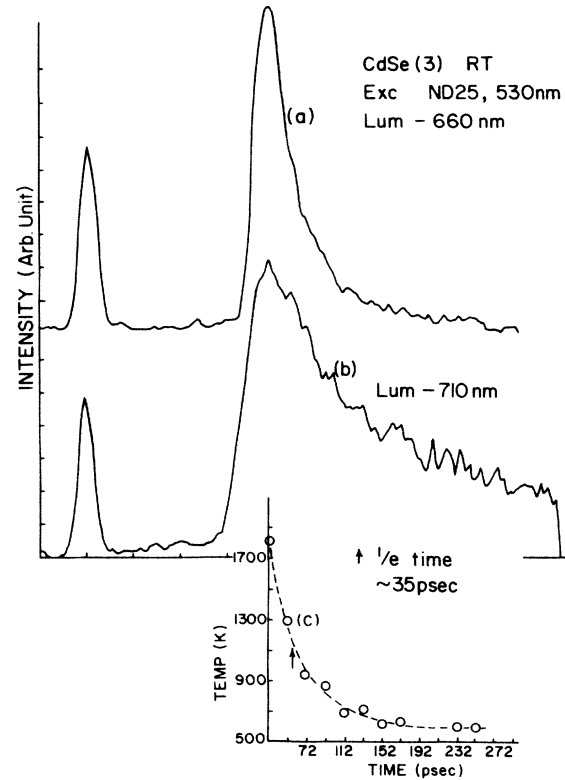


FIG. 9. Curves (a) and (b) correspond to hot (660 nm) and band-edge (710 nm) luminescence from CdSe(3) at a photon fluence $\frac{1}{4}I_F$. The temperature decay profile is obtained from Eq. (36) as shown in the figure.

decay kinetics will be analyzed in terms of Auger recombination^{23,31} to estimate the carrier density. The time-integrated spectra is analyzed in terms of non- k -selection allowed recombination to estimate the carrier density. The excitonic formation time is investigated in terms of the Mott criterion^{28,32} and fast diffusion. The spatial profile broadening of the luminescence was interpreted in terms of fast diffusion. All the experiments at room temperature indicate that the maximum attainable density at the maximum of time-resolved luminescence is $< 2 \times 10^{19}$ cm^{-3} which will be discussed in detail in this section.

VII. HOT-CARRIER ENERGY RELAXATION

The measured delay times are related to the screening of electron-phonon interactions. As we have discussed previously, the initial carrier temperature with our experimental condition (sample CdSe and $\hbar\omega = 2.34$ eV) at $t=0$ is 2560 K. This will be true irrespective of excitation fluences. The temperature of these photogenerated carriers reduces in time due to LO-phonon emission. The temperature measured at the peak of the luminescence corresponds to the net cooling that occurs during the delay time of the luminescence. Since the cooling rate is a function of the carrier density produced at $t=0$, the delay times are different at different excitation fluences. We attribute the large delay time at high-excitation fluence to the reduction of LO-phonon scattering via screening. As it is difficult to estimate the carrier density during the de-

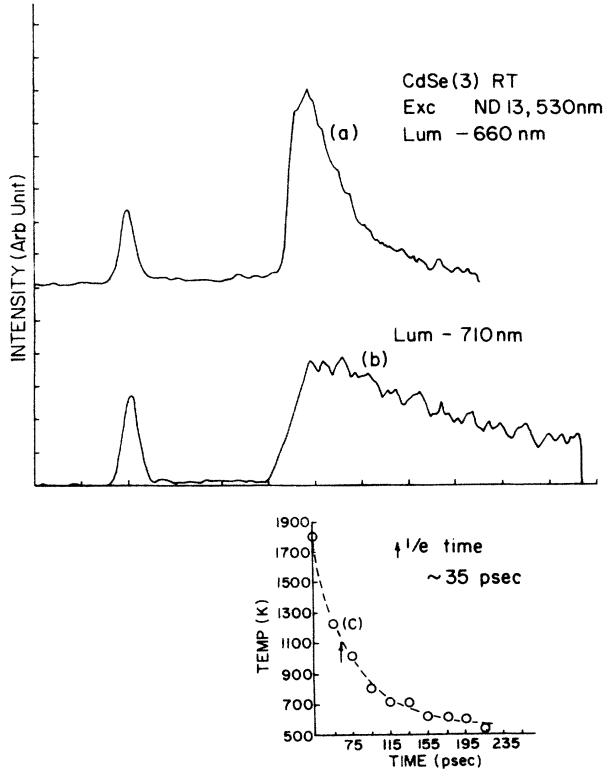


FIG. 10. Curves (a) and (b) correspond to hot (660 nm) and band-edge (710 nm) luminescence from CdSe(3) at photon fluence $\frac{1}{8}I_F$. The temperature decay profile is obtained from Eq. (36).

lay time due to fast diffusion of carriers, we use the delay time and the observed temperature at the peak of luminescence to estimate the average carrier density during the delay time.

The energy relaxation rate can be obtained from the temperature decay profile for times greater than the delay time for a given excitation fluence. This observed rate is compared with the theoretical rate. The difference if any is explained in terms of screening of the electron-phonon interaction by taking into account the carrier density (at time Δt) obtained using the Auger recombination kinetics and the critical density N_c at the temperature under consideration.

A. Screening of electron-phonon interaction and delay time

As a next step using energy-loss rate Eq. (10), the theoretical values of Δt (delay time) will be calculated as follows. For $T_e = 2560$ K ($t=0$), $T_0 \approx 300$ K, $D' = 0.6 \times 10^9$ eV/cm, $\rho = 5.86$ gm/cm³, $\delta = 26$ MeV, and $m_e = 0.13m_0$, we calculate

$$\frac{dE}{dt} = 1.3 \times 10^{10} \text{ eV/sec at } t=0.$$

After 42 psec [CdSe(1) Table I], for maximum excitation fluence, the carrier temperature T_e is ≈ 2100 K [see Fig. 6(c)]. Hence, the energy relaxation rate is

$$\frac{dE}{dt} = 1.2 \times 10^{10} \text{ eV/sec (at } t=46 \text{ psec).}$$

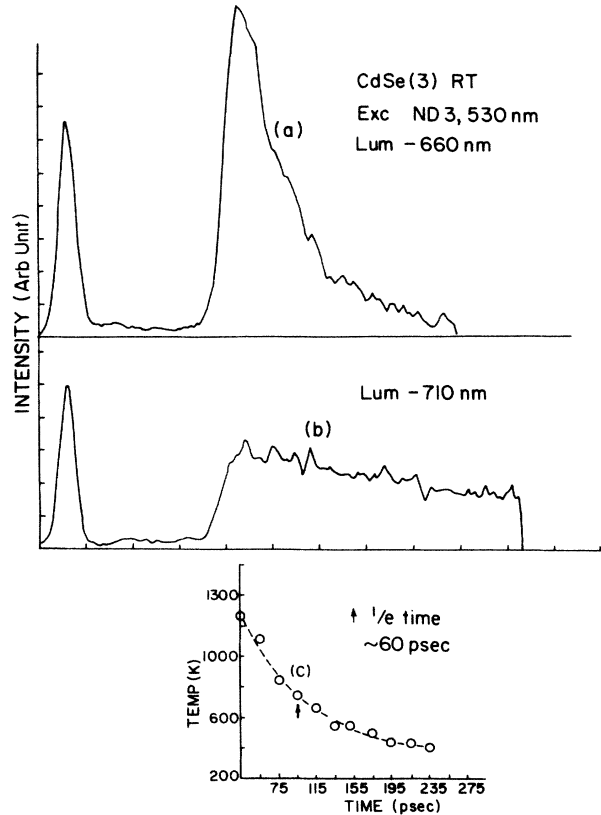


FIG. 11. Curves (a) and (b) represent hot (660 nm) and band-edge (710 nm) luminescence from CdSe(3) at a photon fluence $\frac{1}{33}I_F$. The temperature decay profile is obtained from Eq. (36).

The average rate $\langle dE/dt \rangle$ during the luminescence delay time of 46 psec is $\approx 1.25 \times 10^{10}$ eV/sec. The total energy lost as the electrons cool from 2560 \rightarrow 2100 K is 0.06 eV. With the average rate 1.25×10^{10} eV/sec, the calculated electron (or luminescence) delay time Δt is 5 psec. This does not agree with the observed Δt of 46 ± 5 psec (Table I). The difference between Δt 's we attribute to the screening of electron-phonon interaction since we have used the unscreened (larger) value to determine the average rate. Using Eq. (10) an eightfold decrease is observed in phonon emission rate, giving $N/N_c = \sqrt{7}$. This corresponds to an average carrier density within 46 psec of 2×10^{20} cm⁻³ instead of 3×10^{21} cm⁻³ obtained using Eq. (8). For $\frac{1}{33}I_F$ excitation, the carrier temperature after 27 psec [CdSe(1), Table I, and Fig. 7(c)] is 700 K. The corresponding $\langle dE/dt \rangle$ is 1.1×10^{10} eV/sec and the calculated Δt is 21 psec compared to observed Δt of 27 psec. The carrier density obtained during 27 psec corresponds to 4×10^{19} cm⁻³ [Eq. (10) and 1.3-fold reduction in phonon emission rate] instead of 8.5×10^{19} cm⁻³ [Eq. (8)].

These results clearly show the existence of screening of the electron-phonon interaction during the delay time of luminescence for high-excitation fluence I_F and excitation fluence-dependent fast diffusion of carriers.

The results are similar for CdSe(3) except that the delay times (Table I) and the temperatures [Figs. 8(c), 9(c), 10(c), and 11(c)] at time (ΔT) are consistently larger for the comparable excitation fluences. This indicates more

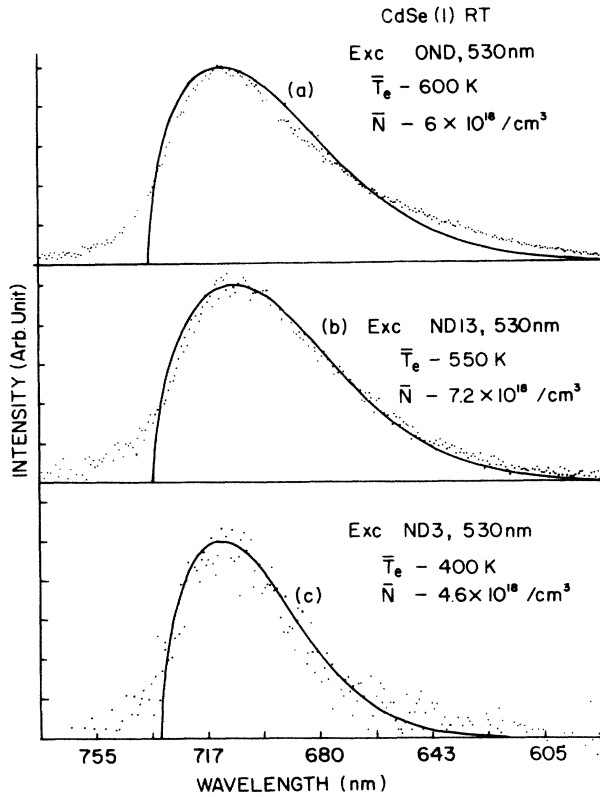


FIG. 12. Time-integrated photoluminescence spectra obtained for various excitation fluences (at 530 nm) in CdSe(1) are shown. The excitation fluence, carrier temperature T_e , and carrier density N are indicated in the figures and were obtained by curve fitting [Eq. (23)] for the parameters listed in the text.

screening in CdSe(3) than in CdSe(1). This is related and consistent with the observed (discussed in Sec. VIII C) smaller “fast diffusion” in CdSe(3), making the average carrier density during Δt larger as compared to that in CdSe(1).

In our experiments the excitation spot size at the sample is ~ 1.35 mm, while the optical-absorption length is $\approx 0.5 \mu\text{m}$. Thus, the longitudinal diffusion of carriers into the surface of the sample controls the carrier density in the photoexcited region due to maximum volume change along the excitation direction (longitudinal). In CdSe(1) the c axis is coincident with the longitudinal direction, while in CdSe(3) the c axis is perpendicular to the longitudinal direction. The latter constant along the c axis and perpendicular to the c axis are ≈ 7 and 4 Å, respectively,

TABLE II. Carrier temperatures and carrier densities obtained from theoretical fittings to the experimentally observed spectra are shown for CdSe(1) at various excitation fluences.

Excitation intensity (photons/cm ²)	Carrier density \bar{N} (cm ⁻³)	Carrier temperature T_e (K)
I_F	6.0×10^{18}	600
$\frac{1}{8} I_F$	7.2×10^{18}	550
$\frac{1}{33} I_F$	4.6×10^{18}	400

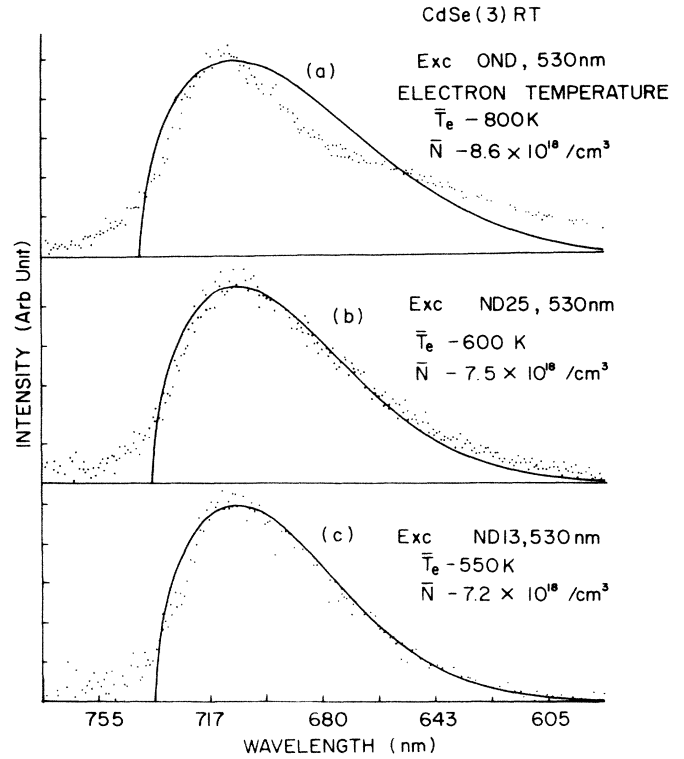


FIG. 13. Time-integrated photoluminescence spectra obtained for various excitation fluences (at 530 nm) in CdSe(3) are shown. The excitation fluence, carrier temperature T_e , and carrier density N are indicated in the figures. The continuous lines are theoretical fits [Eq. (23)].

making the mean collision time (unscreened) larger in the previous case as compared to the latter. This fact qualitatively explains the larger diffusion constant in CdSe(1) making a smaller $N(\Delta t)$ (by a factor of 2) compared to CdSe(3).

B. Screening of electron-phonon interaction and temperature decay time

The temperature (or energy) relaxation rate obtained from Fig. 6(c) is 0.3×10^{19} eV/sec, while the rate calculated using Eq. (10) is 0.9×10^{10} eV/sec at 1700 K. This difference is due to the screening of the electron-phonon interaction. For carriers having a temperature of 1700 K [average temperature during 35 psec on the decay profile Fig. 6(c) or $E_i \sim 0.21$ eV], one calculates, using Eqs. (6)

TABLE III. Carrier temperatures and carrier densities obtained from theoretical fittings to the experimentally observed spectra are shown for CdSe(3) at various excitation fluences.

Excitation intensity (photons/cm ²)	Carrier density \bar{N} (cm ⁻³)	Carrier temperature T_e (K)
I_F	8.6×10^{18}	800
$\frac{1}{4} I_F$	7.5×10^{18}	600
$\frac{1}{8} I_F$	4.6×10^{18}	500

and (3), the critical density N_c to be $2 \times 10^{19} \text{ cm}^{-3}$. The experimentally determined carrier density at the peak of the luminescence (Table I) is $2 \times 10^{19} \text{ cm}^{-3}$. At this density the phonon emission rate will be reduced by a factor of 2, i.e., $0.45 \times 10^{10} \text{ eV/sec}$. This value is close to the observed value of $0.3 \times 10^{10} \text{ eV/sec}$.

The temperature decay data [Fig. 7(c)] obtained for $\frac{1}{33}I_F$ excitation cannot be analyzed in terms of Eq. (10) as the carriers are cooled to the lattice temperature ($\approx 400 \text{ K}$) and the LO-phonon emission process is no longer efficient. The data [Figs. 8(c), 9(c), 10(c), and 11(c)] obtained for CdSe(3) also shows screening over the entire range of excitation fluences. This again indicates that the carrier densities are higher in CdSe(3) than in CdSe(1) due to "less" fast diffusion as compared to CdSe(1).

The possibility of reduction in the cooling rate of hot photoexcited carriers due to phonon reabsorption can be eliminated on the following grounds. If we assume a typical Debye heat capacitance,³³ i.e., $25 \text{ J mol}^{-1} \text{ K}^{-1}$ for $T > \Theta$, where Θ , is the Debye temperature (for CdSe $\approx 315 \text{ K}$), then for the maximum energy deposited of $400 \mu\text{J/pulse}$, we obtain a maximum lattice temperature rise of 150 K assuming a quantum efficiency of 10% (radiative lifetime $\approx 2 \text{ nsec}$ and observed lifetime of $\approx 200 \text{ psec}$). In the above estimate, we assume that the phonons remain within the initial absorption depth $\approx 10^{-4} \text{ cm}$. This is an overestimate as the phonon lifetime of $\approx 5 \text{ psec}$ has not been taken into account. Thus, carrier heating due to phonon absorption by the carriers is a negligible effect making the phonon bottleneck mechanism inefficient.

C. Estimates of effective diffusion constant

The measured delay times and carrier densities (using Auger kinetics) can be used to estimate an effective diffusion constant D_t at different average photogenerated carrier densities during the delay times. The effective D_t is given by

$$D_{t,\text{eff}} = \left[\frac{N}{\alpha N(\Delta t)} \right]^2 \left[\frac{1}{4\pi\Delta t} \right], \quad (37)$$

where N is given by Eq. (8) and $N(\Delta t)$ is obtained from the Auger analysis which is listed in Table IV for various excitation fluences. The values of Δt are listed in Table I [CdSe(3)]. Thus, neglecting carrier recombination, the effective values of D_t obtained at the surface ($x=0$) are 2.2×10^4 , 2×10^3 , 5×10^2 , and $60 \text{ cm}^2/\text{sec}$ for I_F , $\frac{1}{4}I_F$, $\frac{1}{8}I_F$, and $\frac{1}{33}I_F$, respectively.

TABLE IV. Auger recombination rates and carrier densities are obtained from fittings to the time-resolved luminescence [Eq. (13)] at various excitation fluences.

Excitation intensity (photons/cm)	Auger rate (sec^{-1})	Carrier density N (cm^{-3})
I_F	4.5×10^9	2×10^{19}
$\frac{1}{4}I_F$	2.5×10^9	1.6×10^{19}
$\frac{1}{8}I_F$	2.5×10^9	1.5×10^{19}
$\frac{1}{33}I_F$	1.5×10^9	1.2×10^{19}

$\frac{1}{8}I_F$, and $\frac{1}{33}I_F$ excitation fluences, respectively. Since $N(\Delta t)$ depends on the Auger recombination constant C [$N(\Delta t) \approx 1/\sqrt{C}$] the effective D_t will depend on the choice of C . We have shown data of $D_{t,\text{eff}}$ for two values of C in Fig. 3. It is difficult to estimate C as the carrier temperature varies rapidly during Δt [Fig. 6(c)]. However, the data shows the same dependence for a large range of D_t at high-carrier densities.

VIII. DIRECT EXPERIMENTAL EVIDENCES FOR FAST DIFFUSION

A. Time-integrated spectra

From this study we were able to estimate directly average photogenerated carrier density and temperature at different excitation fluences. The moderate change in the estimated carrier density is due to rapid reduction in the carrier density within the thermalization period. At a maximum excitation intensity of $7 \times 10^{16} \text{ photons/cm}^2$, the theoretical fit to the time-integrated luminescence spectra is not good [Fig. 12(a)]. The reason is because the temperature decay profile has two components at these high excitation fluences [see Fig. 6(c) for CdSe(1) and 6(c) for CdSe(3)]. Due to screening of the electron-phonon interaction, the high-energy side of the time-integrated spectra shows two components corresponding to these two temperature regimes. But for lower excitation intensities there is an excellent agreement between the theoretical fit and data for the parameters shown in Figs. 12(b) and 12(c). It should be noted that the average electron temperature and the carrier density obtained are slightly larger for higher excitation power (see Table II).

For CdSe(3), the observed temperatures and carrier densities are higher than observed in CdSe(1) for the comparable excitation powers (see Table III). Since the dynamic range of sensitivity for our vidicon detection is from the maximum fluence I_F to the minimum $\frac{1}{33}I_F$ excitation and since the photoluminescence lifetime ($1/e$) is 230 psec , the integrated photoluminescence spectra obtained is an average over a maximum time duration of about 800 psec for full intensity and 500 psec for $\frac{1}{8}I_F$ excitation. The time-resolved photoluminescence study shows that the hot-carrier cooling occurs within 100 psec . Therefore, we can assume the carriers remain at a constant hot temperature for the next 100 – 800 psec . Thus the temperature obtained from the theoretical fit of the time-integrated photoluminescence is a good indicator of the average hot-carrier temperature.

The entire photoexcitation fluence range I_F to $\frac{1}{33}I_F$ covered in the experiment has only a moderate effect on the final carrier temperature and average Fermi energy (average carrier density). This observation strongly suggests longitudinal (bulk) fast diffusion of carriers away from the surface and from the photoexcited region. The reasons, why the longitudinal and not the transverse (within the surface irrespective of c -axis orientation) diffusion affects the carrier density, were discussed earlier. The carrier densities observed in CdSe(1) are less than the ones observed in CdSe(3). The only difference in the experimental condition between these samples is that the

longitudinal diffusion occurs along the c axis in CdSe(1) while, it is perpendicular to the c axis in CdSe(3). This difference in the carrier densities suggests that diffusion along the c axis is larger than along the perpendicular direction by a factor of 1.3.

The carrier densities measured by the time-integrated spectra experiment are the average densities (over ≈ 500 psec). Hence, if we correct them for the luminescence decay time of 230 psec, the carrier densities at the peak of the luminescence are 4.4×10^{19} , 5.3×10^{19} , and 3.4×10^{19} cm^{-3} for I_F , $\frac{1}{8}I_F$, and $\frac{1}{33}I_F$ excitation fluences, respectively. Similarly in CdSe(3) the initial carrier densities (maximum of luminescence) are 6.3×10^{19} , 5.5×10^{19} , and 3.4×10^{19} cm^{-3} for I_F , $\frac{1}{4}I_F$, and $\frac{1}{8}I_F$ excitation fluences, respectively. These values of carrier densities are quite consistent with the ones obtained in Sec. VIII B.

B. Auger recombination of carriers

The time-resolved band-edge (710 nm) luminescence from CdSe(3) displays (Fig. 14) a fast component of ≈ 35 psec (τ_1) and a slow component of 230 psec (τ_2) which was fitted by

$$L(t) = A_1 \exp(-t/\tau_1) + A_2 \exp(-t/\tau_2) \quad (38)$$

for t in psec. Such a double exponential analysis does not carry any physical meaning. We have analyzed the data

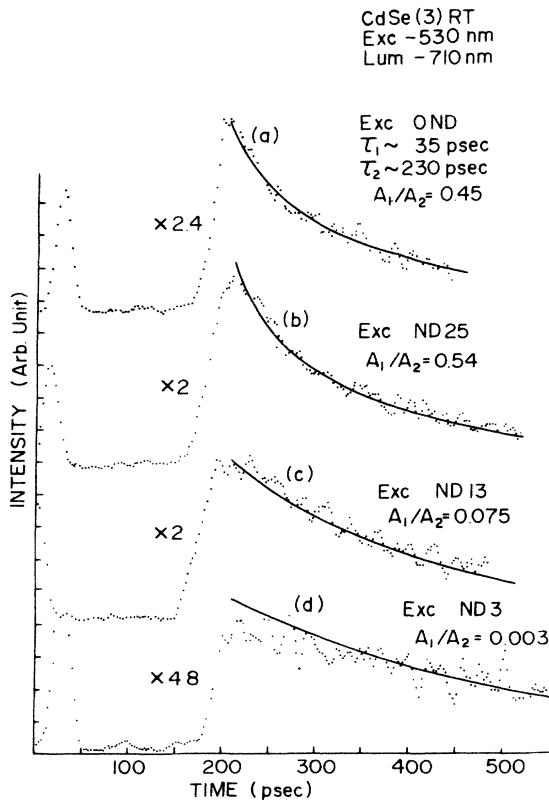


FIG. 14. Time-resolved photoluminescence at 710 nm obtained from CdSe(3) at various photon fluences are shown. The continuous lines are double exponential fits [Eq. (38)] with time constants 35 and 230 psec. The ratios A_1/A_2 for the curves (a), (b), (c), and (d) are as shown in the figure.

with Eq. (38) just to rule out a possibility of intervalence-band transition and relate the intensity dependence of A_1/A_2 to Auger recombination [Eq. (13) and Fig. 15]. The ratio A_1/A_2 for excitation intensities of $4I_F$, I_F , $\frac{1}{2}I_F$, and $\frac{4}{33}I_F$ are 0.45, 0.54, 0.075, and 0.003, respectively.

In this experiment the excitation photon polarization was set parallel ($E \parallel C$) to the c axis. The photoluminescence collected was not discriminated for polarization nor for the terminal valence-band states Γ_9 and Γ_7 due to the choice of the broad-band filter (R70) in front of the streak camera. In this geometry the holes are created only in the B valence band at $t=0$. The fast component observed could arise from either to a fast scattering (say, 35 psec) from Γ_7 (B valence) band to Γ_9 (A valence) band or due to the Auger recombination²³ of carriers.

The possibility of hole scattering ($\Gamma_9 - \Gamma_7$) is excluded for the five following reasons.

(i) The initial ($t=0$) energy E_i^B of holes in B valence band is given by

$$E_i^B = (\hbar\omega_1 - E_g) \frac{m_e}{m_h^B + m_e}, \quad (39)$$

where $m_h^B = m_0$ is the effective mass of B (Γ_7) holes, $m_e = 0.13m_0$, and $E_g^B = E_g^A + 0.026 = 1.736$ eV ($\Delta_{cr} = 0.026$ eV). Thus, for 2.34-eV one-photon excitation (530 nm) E_i^B is 70 meV. The total scattering of holes from B valence to A valence band is due to nonpolar LO-phonon emission and to acoustical phonon emission.

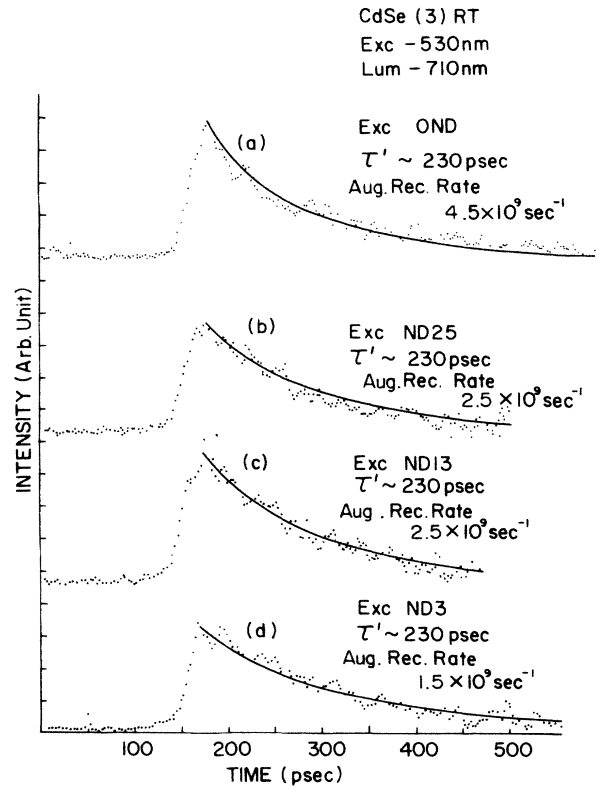


FIG. 15. Experimental data obtained under similar experimental conditions as that of Fig. 14 but with a maximum excitation fluence of $4I_F$. The continuous lines are fits to Eq. (13) with recombination rates shown in the figure using $C = 1 \times 10^{-29} \text{ cm}^{-6} \text{ sec}^{-1}$.

phonon emission and to acoustical phonon emission.

The acoustical phonon scattering rate is given by¹⁶

$$\frac{dE}{dt} = -8\sqrt{2}/(\pi^{3/2}) \frac{E_1^2 m^{(5/2)}}{\hbar^4 \rho} (kT_e)^{3/2} \left[1 - \frac{T_0}{T_e} \right], \quad (40)$$

where $E_1 = 5.7$ eV is the acoustical deformation potential.^{16,21} For $m = m_h^B$, $T_0 = 300$ K, and $T_e = T_h = 2000$ K, the estimated value is

$$\left\langle \frac{dE}{dt} \right\rangle = 2.1 \times 10^{10} \text{ eV/sec}.$$

Therefore, the total scattering time for emitting 100-meV energy from $\Gamma_7 \rightarrow \Gamma_9$ will occur in ≈ 1 psec. This is contrary to the observed decay time of 35 psec.

One should note that Yoshida *et al.*²⁹ had observed a scattering time of 35 psec for $\Gamma_7(B) \rightarrow \Gamma_9(A)$ hole scattering at 4 K. The carrier density in their experiment was $\approx 3 \times 10^{17} \text{ cm}^{-3}$ and the carrier temperature T_e was low ≈ 30 K. If one takes into account these facts, this should explain their measured scattering time of 35 psec within the framework of nonpolar LO- and acoustical phonon emission given above.

(ii) The B valence-band holes are scattered into the A valence band. Since the luminescence of B and A valence bands are observed simultaneously there should not be an added fast component to the luminescence decay.

(iii) The ratio of density of states of A valence and B valence is given by

$$\frac{N_A}{N_B} = \left[\frac{m_A}{m_B} \frac{E_i^A}{E_i^B} \right]^{3/2}. \quad (41)$$

Since m_A and m_B are $0.45m_0$, and m_0 , respectively, and $E_i^A = 140$ meV and $E_i^B = 70$ meV; therefore

$$\frac{N_A}{N_B} = 0.85. \quad (42)$$

Hence, the observed A_1/A_2 ratio should be $\approx > 1$ compared to the observed ratio of $\ll 1$ (see Fig. 14).

(iv) The observed time-resolved photoluminescence kinetics is intensity dependent.

(v) For CdSe(3), if the excitation photon polarization is perpendicular to the c axis (the c axis is still in the plane) the same kinetics is observed. This is the most important observation since in this geometry of excitation both A and B bands are pumped and the scattering from B to A would be diminished. However, no fast component is observed in CdSe(1) for the same excitation polarization (the c axis is perpendicular to the plane). These observations together support the strong Auger recombination²³ in CdSe(3) due to the presence of high-carrier density (less diffusion) after the thermalization time of ≈ 30 psec.

After excluding the above five possibilities, the Auger recombination²³ is considered to be responsible to the fast decay [Eqs. (11), (12), and (13)].

The time-resolved luminescence at various pump intensities [Fig. 15] were analyzed using Eq. (13) and $C = 1 \times 10^{-29} \text{ cm}^{-6} \text{ sec}^{-1}$. In CdSe(1), we do not see the Auger recombination component (absence of fast component in Fig. 4, even for the maximum photon fluence

I_F . This suggests that the fast component is longer than the 460 psec (or rate $< 1 \times 10^9 \text{ sec}^{-1}$), the monomolecular lifetime of carriers. This indicates that for the whole excitation fluence range I_F to $\frac{1}{33} I_F$ the carrier densities generated are less than $1 \times 10^{19} \text{ cm}^{-3}$. On the contrary, in CdSe(3), the observed Auger recombination (Fig. 15 fast component) indicates carrier densities $> 1.0 \times 10^{19} \text{ cm}^{-3}$ (Table IV) but $< 2.0 \times 10^{19} \text{ cm}^{-3}$. The longitudinal fast diffusion, within 35 psec, away from the photoexcited surface could limit the initial carrier density in our experiment due to limited time resolution. In CdSe(1), the c axis is perpendicular to the surface and in CdSe(3), the c axis lies in the surface. Hence, we can conclude that the fast diffusion along the c axis is greater than that along the perpendicular direction by a factor of 2.

C. Exciton formation from dense $e-h$ plasma

The exciton formation from a dense free $e-h$ plasma occurs when the plasma density becomes equal or to less than the Mott density.^{28,32} This can be used to estimate the initial free $e-h$ plasma density.

The laser pulse, having a photon energy greater than the band gap, first creates a free-electron hole pair which thermalizes and finally dissipates the excess energy to the lattice through LO- and acoustical phonon emission. During the energy relaxation process, reduction in the carrier density occurs due to recombination and plasma expansion. Exciton formation occurs as a result of the Coulomb interaction between electrons and holes provided that the $e-h$ plasma density is sufficiently low and lattice thermal energy is less than the exciton binding energy.

The criterion for this Mott transition which separates the conducting plasma state and the "insulating" excitonic state is that the carrier density should not be able to screen the Coulomb interaction between the $e-h$ pair. The Mott criterion^{28,32} is written as

$$N_m^{1/3} a_x = 0.2, \quad (43)$$

where a_x is the Bohr radius for an exciton and N_m is the number density of the $e-h$ plasma. For CdSe, with $a_x \sim 40$ Å, this yields a Mott density of $N_m = 1 \times 10^{17} \text{ cm}^{-3}$.

When the laser pulse photogenerates a carrier density $N > N_m$ there is a time delay between the onset of exciton formation and the laser pulse. For the entire (intensity detection limited) one-photon excitation fluence range, the photogenerated carrier density $N \gg N_m$. In order to overcome this difficulty two-photon excitation was used. This method yielded a larger photoluminescence even though the carrier density was low. This is due to the larger penetration depth which reduces surface recombination compared to one-photon excitation.

The carrier density for two-photon absorption was calculated as follows:³⁴

$$\frac{dI(z)}{dz} = -[\alpha + \beta I(z)]I(z), \quad (44)$$

where $I(z)$ is the intensity of the laser in the sample at depth z measured from the incident surface, α is the one-photon absorption coefficient ($\alpha \approx 0.18 \text{ cm}^{-1}$) at 1060 nm

and β is the two-photon absorption coefficient ($\beta \approx 0.03$ cm/MW) at 1060 nm. For the laser power > 1 GW/cm² (pulse), the one-photon absorption at 1060 nm (Nd:glass-laser fundamental wavelength) could be neglected in comparison to two-photon absorption. In this case Eq. (44) reduces to

$$\frac{1}{I(z)} = \frac{1}{I_0} + \beta z, \quad (45)$$

where I_0 is the incident intensity at the surface ($z=0$). The reduction in intensity $\Delta I = (I_0 - I)$ is

$$\Delta I = \frac{\beta z I_0^2}{1 + \beta z I_0}. \quad (46)$$

As the luminescence observed emerges from a crystal depth of ≈ 1 μ m (due to reabsorption near band gap), we can conclude the average carrier density within 1 μ m of the surface assuming ΔI is converted into $e-h$ plasma. For the maximum I_0 of 7 GW/cm²,

$$\Delta I = 144 \text{ MW/cm}^2.$$

For a pulse duration of 5 psec the maximum carrier density produced is 2×10^{19} cm⁻³. For 10% attenuation of I_0 with an ND25, $\Delta I = 1.44$ MW/cm² and the carrier density is 2×10^{17} cm⁻³.

For I_0 excitation, the initial ($t=0$) estimated carrier density is 2×10^{19} cm⁻³ and the photoluminescence lifetime [Fig. 16, curve (a)] is ≈ 120 psec. The time required for the density to go down by a factor of 200 to reach the Mott density 1×10^{17} cm⁻³ will be ≈ 600 psec. Hence, the observed excitonic luminescence will be delayed in time to ≈ 600 psec after the laser excitation pulse. This is outside the decay range and was not observed [Fig. 16, curve (a)]. However, the experimentally observed time-resolved excitonic peak occurs after 185 psec (i.e., the Mott density is reached after 185 psec [see Fig. 16, curve (c)]. This fact leads us to believe that the carrier density achieved after laser pulse with I_0 excitation intensity is $\approx 5 \times 10^{17}$ cm⁻³ and not equal to the calculated value of 2×10^{19} cm⁻³.

With $\frac{1}{10} I_0$ excitation, however, the excitons are formed almost instantly as the initial carrier density is about 2×10^{17} cm⁻³. Experimentally one can see [Fig. 16, curve (a)] that the free plasma peak with one-photon excitation is separated from the prepulse by 105 psec while the excitonic peak is separated by 118 psec [Fig. 16, curve (b)]. The free plasma luminescence cannot be observed along with the exciton luminescence because of the low quantum yield in the previous case (the exciton luminescence is strong compared to the free $e-h$ plasma luminescence and is separated by ≈ 50 Å and cannot be discriminated by a broad-band filter).

To account for the reduction of carrier density one needs a large diffusion constant. An effective diffusion coefficient $D_t = 4.2 \times 10^4$ cm²/sec is estimated using Eq. (37), the initial density at $t=0$ of 2×10^{19} cm⁻³, and final density of 5×10^{17} cm⁻³. Hence, the $e-h$ plasma expands over a length of 40 μ m after 30 psec (thermalization time of free $e-h$ plasma) to yield a density of 5×10^{17} cm⁻³.

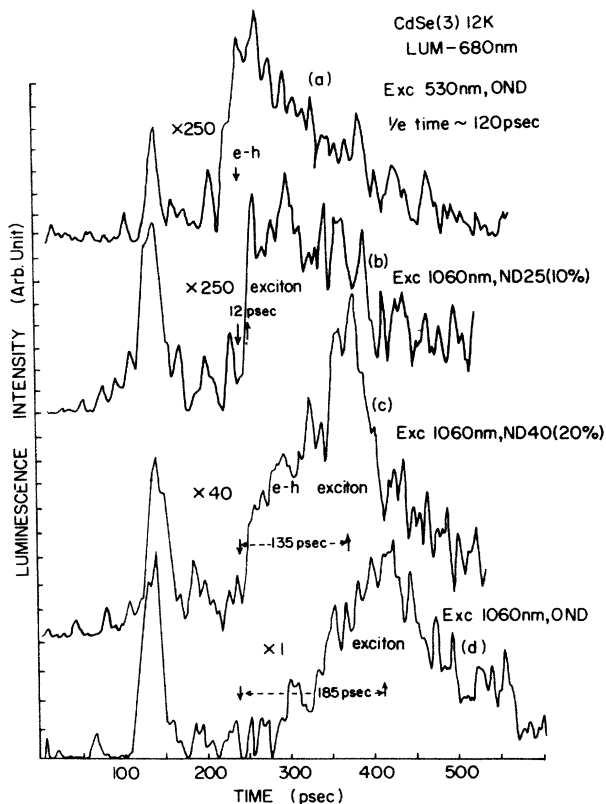


FIG. 16. Curve (a) represents free $e-h$ plasma luminescence at 12 K from CdSe(3) obtained with 530-nm excitation. Curve (b) corresponds to exciton luminescence obtained with two-photon excitation attenuated by 10% of the maximum used in curve (d). The exciton luminescence peak is [shown in curve (d)] delayed by 185 psec.

D. Time-integration spatial profile

Using the streak camera in the focus mode we were able to measure the laser spatial profile and the luminescence spatial profile at the sample [CdSe(1)]. The time-integrated spatial profiles of the luminescence differ greatly in width (FWHM) as compared to the laser spatial profile. The photoluminescence profile was integrated over a time duration of 1 nsec (due to the dynamic range) and clearly shows a transverse diffusion of carriers within 1 nsec. The laser width was 1.35 mm while the photoluminescence width was ≈ 2.19 mm [see Fig. 17] at the sample. The estimate of the transverse velocity assuming that the luminescence is collected during 1 nsec, is 4×10^7 cm/sec (velocity needed for plasma to expand through 0.42 mm in 1 nsec). The transverse diffusion does not contribute to the drastic reduction of carrier density within the thermalization time (≈ 30 psec). This is due to the fact that the laser beam profile at the sample is focused down to 1.35-mm diameter (1350 μ m) as compared to the absorption depth for one-photon absorption (2.34 eV) of 0.5 μ m. However, it can easily be seen that in our experiments with the lower limit on the velocities of 4×10^7 cm/sec, the carriers initially generated within 0.5 μ m will diffuse to 12 μ m within 30 psec (delay time). This reduces the density by a factor of 25. If the satur-

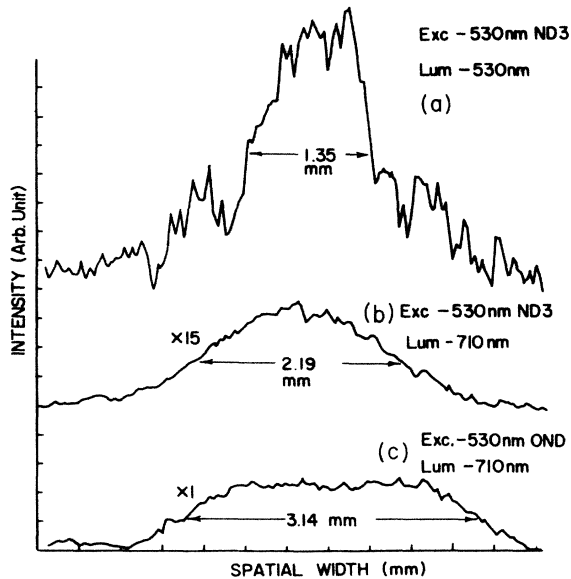


FIG. 17. Curve (a) shows the laser spatial profile of 530-nm excitation. Curves (b) and (c) are the spatial profiles of 710-nm luminescence obtained over a period of 1 nsec after the pulse excitation. The FWHM of the profiles are shown in the figure.

tion of states is the reason for the observed broader luminescence profile instead of fast diffusion (the wings of the laser profile has enough power to generate the same carrier density as at the center), i.e., 0.85 mm over the laser profile for $\frac{1}{33}I_F$ excitation, then the luminescence spatial profile would be 27 mm over the laser profile for I_F excitation. This is contrary to the observed increase of 1.79 mm (Fig. 17).

IX. CONCLUSION

Rapid diffusion of high-density nonequilibrium photo-generated carrier with diffusion constant largely exceeding the typical equilibrium values can account for moderate intensity dependence of the Auger recombination of free carriers and of the carrier Fermi level in the time-integrated spectra at room temperature. Such a rapid diffusion can also account for exciton formation at high excitation intensities and the increased photoluminescence

spatial profile over that of the laser profile. We conclude that the maximum carrier density attainable by one-photon excitation at room temperature is $\approx 1 \times 10^{19} \text{ cm}^{-3}$ after 30 psec. This limit is further reduced to $5 \times 10^{17} \text{ cm}^{-3}$ at low temperature and is due to the fast diffusion of carriers and not due to the saturation of absorbing states. Comparing the time-resolved decay curves for CdSe(1) and CdSe(3), which shows absence of Auger recombination in the previous case, makes us believe that the diffusion velocities along the c axis are greater than along the perpendicular direction by a factor of 2. This results in rapid diffusion within 30 psec reducing the initial carrier density in CdSe(1) more than in CdSe(3) with its c axis parallel to the plane.

The possibility of reradiation and reabsorption is ruled out since a process will shift the luminescence to the red (high-energy tail will be absorbed more). The temperature cooling rate obtained from the time-resolved, hot and band-edge luminescence, would be faster yielding much lower temperatures after ≈ 30 psec for high pump intensities. This is contrary to the observation. Such a mechanism is more important for ultrathin samples as compared to bulk. Also the luminescence from the samples was collected in a frontal geometry reducing the self-absorption. In addition, this process will make lifetimes longer with increasing pump intensity in contrast to observation.

Within the theoretical framework of screening of the electron-phonon interaction, we conclude from our experiments that the nonpolar optical-phonon emission due to the optical deformation potential is the dominant energy relaxation mechanism. The rapid diffusion of carriers due to the screening of electron-phonon interaction is an important phenomenon in limiting the photogenerated carriers and should be taken into account in refining the existing treatise of high-density energy and spin relaxation.¹⁵

ACKNOWLEDGMENTS

We thank Dr. Nathan Ockman for helpful comments on the manuscript. We thank Dr. Marina Foresti and Mr. W. B. Wang for technical assistance. The research was funded by the U.S. Air Force Office of Scientific Research, National Science Foundation Grant No. DMR-840-4932, and through Professional Staff Congress and Board of Higher Education grants at the City University of New York.

¹R. Ulbrich, Phys. Rev. 8, 5719 (1973).

²J. Shah, Phys. Rev. B 9, 562 (1974).

³E. O. Gobel and O. Hildebrand, Phys. Status Solidi B 88, 645 (1978).

⁴Since, $\frac{3}{2}k_B T_e + \frac{3}{2}k_B T_h = \frac{3}{2}k_B(T_e + T_h) = \Delta E$ and $T_e = T_h = T_i$, $\frac{3}{2}k_B(2T_i) = (\hbar\omega_l - E_g)$.

⁵E. J. Yoffa, Phys. Rev. B 21, 2415 (1980).

⁶B. R. Nag, *Semiconductors Probed by Ultrafast Laser Spectroscopy*, edited by R. R. Alfano (Academic, New York, 1984), Vol. 1, pp. 3–43.

⁷C. J. Hearn, Proc. Phys. Soc. 86, 881 (1965).

⁸A. Cornet, M. Pugnet, J. Collet, T. Amand, and M. Brousseau,

J. Phys. (Paris) Colloq. C7-471 (1981).

⁹M. Combescot, Solid State Commun. 30, 81 (1979).

¹⁰R. Zimmerman and M. Rosler, Phys. Status Solidi B 75, 633 (1976).

¹¹K. M. Romanek, H. Nather, J. Fischer, and E. O. Gobel, J. Lumin. 24/25, 585 (1981).

¹²S. Modesti, L. G. Quaglino, A. Frova, J. L. Staehli, and M. Guzzi, J. Lumin. 24/25, 581 (1981).

¹³A. Forchel, H. Schweizer, and G. Mahler, Phys. Rev. Lett. 51, 501 (1983).

¹⁴E. J. Yoffa, Phys. Rev. B 23, 1909 (1981).

¹⁵H. Frohlich, Proc. R. Soc. London, Ser. A 160, 230 (1937).

- ¹⁶E. M. Conwell, *High Field Transport in Semiconductors* (Academic, New York, 1967).
- ¹⁷A. R. B. de Castro and R. S. Turtelli, *Solid State Commun.* **32**, 819 (1979).
- ¹⁸J. I. Pankove, *Optical Processes in Semiconductors* (Dover, New York, 1975), p. 6.
- ¹⁹Cleveland Crystal Information Sheet (19306 Redwood Ave, Cleveland, Ohio, 44110), June 1980.
- ²⁰R. B. Parsons, R. B. Wardzynski, and A. D. Yoffe, *Proc. R. Soc. London, Ser. A* **262**, 120 (1961).
- ²¹M. Pagnet, J. Collet, and A. Cornet, *Solid State Commun.* **38**, 531 (1981).
- ²²M. R. Junnarkar, R. R. Alfano, and J. Furdyna (unpublished).
- ²³J. S. Blackmore, *Semiconductor Statistics* (Pergamon, New York, 1962), p. 214.
- ²⁴M. Takeshima, *Phys. Rev. B* **23**, 6625 (1981).
- ²⁵S. S. Yao and R. R. Alfano, *Phys. Rev. B* **27**, 1180 (1983).
- ²⁶E. J. Yoffa, *Appl. Phys. Lett.* **36**, 37 (1980).
- ²⁷R. A. Smith, *Semiconductors* (Cambridge University Press, Cambridge, England, 1961).
- ²⁸N. J. Frigo, H. Mahr, and D. J. Erskine, *IEEE J. Quantum Electron.* **QE-18**, 192 (1982).
- ²⁹H. Yoshida, M. Saito, and S. Shionoya, *J. Phys. Soc. Jpn.* **50**, 881 (1981).
- ³⁰P. Y. Lu, P. P. Ho, and R. R. Alfano, *J. Quantum. Electron.* **QE-15**, 406 (1979).
- ³¹A. Haug, *Solid State Electron.* **21**, 1281 (1978).
- ³²N. Mott, *Philos. Mag.* **6**, 287 (1961).
- ³³C. Kittel, *Introduction to Solid State Physics*, 5th ed. (Wiley Eastern University, New York, 1977), p. 136.
- ³⁴A. F. Stewart and M. Bass, *Appl. Phys. Lett.* **37**, 1040 (1980).
- ³⁵M. R. Junnarkar, R. R. Alfano, and J. Furdyna (unpublished).